8 Quantum Monte Carlo methods

8.1 INTRODUCTION

In most of the discussion presented so far in this book, the quantum character of atoms and electrons has been ignored. The Ising spin models have been an exception, but since the Ising Hamiltonian is diagonal (in the absence of a transverse magnetic field), all energy eigenvalues are known and the Monte Carlo sampling can be carried out just as in the case of classical statistical mechanics. Furthermore, the physical properties are in accord with the third law of thermodynamics for Ising-type Hamiltonians (e.g. entropy S and specific heat vanish for temperature $T \to 0$, etc.) in contrast to the other truly classical models dealt with in previous chapters (e.g. classical Heisenberg spin models, classical fluids and solids, etc.) which have many unphysical low temperature properties. A case in point is a classical solid for which the specific heat follows the Dulong–Petit law, $C = 3Nk_B$, as $T \to 0$, and the entropy has unphysical behavior since $S \to -\infty$. Also, thermal expansion coefficients tend to non-vanishing constants for $T \to 0$ while the third law implies that they must be zero. While the position and momentum of a particle can be specified precisely in classical mechanics, and hence the groundstate of a solid is a perfectly rigid crystal lattice (motionless particles localized at the lattice points), in reality the Heisenberg uncertainty principle forbids such a perfect rigid crystal, even at $T \to 0$, due to zero point motions which 'smear out' the particles over some region around these lattice points. This delocalization of quantum-mechanical particles increases as the atomic mass is reduced; therefore, these quantum effects are most pronounced for light atoms like hydrogen in metals, or liquid helium. Spectacular phenomena like superfluidity are a consequence of the quantum nature of the particles and have no classical counterpart at all. Even for heavier atoms, which do not show superfluidity because the fluid–solid transition intervenes before a transition from normal fluid to superfluid could occur, there are genuine effects of quantum nature. Examples include the isotope effects (remember that in classical statistical mechanics the kinetic energy part of the Boltzmann factor cancels out from all averages, and thus in thermal equilibrium no property depends explicitly on the mass of the particles).

The quantum character of electrons is particularly important, of course, since the mass of the electron is only about 1/2000 of the mass of a proton, and phenomena like itinerant magnetism, metallic conductivity and superconductivity completely escape treatment within the framework of classical statistical mechanics. Of course, electrons also play a role for many problems of

'chemical physics' such as formation of hydrogen bonds in liquid water, formation of solvation shells around ions, charge transfer in molten oxides, etc. While some degrees of freedom in such problems can already be treated classically, others would still need a quantum treatment. Similarly, for many magnetic crystals it may be permissible to treat the positions of these ions classically, but the quantum character of the spins is essential. Note, for example, in low-dimensional quantum antiferromagnets the Néel state is not the groundstate, and even understanding the groundstate of such quantum spin systems may be a challenging problem.

There is no unique extension of the Monte Carlo method as applied in classical statistical mechanics to quantum statistical mechanics that could deal well with all these problems. Instead, different schemes have been developed for different purposes: for example, the path integral Monte Carlo (PIMC) technique works well for atoms with masses which are not too small at temperatures which are not too low, but it is not the method of choice if groundstate properties are the target of the investigation. Variational Monte Carlo (VMC), projector Monte Carlo (PMC), and Green's function Monte Carlo (GFMC) are all schemes for the study of properties of many-body systems at zero temperature. Many of these schemes exist in versions appropriate to both off-lattice problems and for lattice Hamiltonians. We emphasize at the outset, however, that important aspects are still not yet satisfactorily solved, most notably the famous 'minus sign problem' which appears for many quantum problems such as fermions on a lattice. Thus many problems involving the quantum statistical mechanics of condensed matter exist, that cannot yet be studied by simulational methods, and the further development of more powerful variants of quantum Monte Carlo methods is still an active area of research. (Indeed we are rather lucky that we can carry out specific quantum Monte Carlo studies, such as path integral simulations described in the next section, at all.) The literature is voluminous and has filled several books (e.g. Kalos, 1984; Suzuki, 1986; Doll and Gubernatis, 1990; Suzuki, 1992), and review articles (Ceperley and Kalos, 1979; Schmidt and Kalos, 1984; de Raedt and Lagendijk, 1985; Berne and Thirumalai, 1986; Schmidt and Ceperley, 1992; Gillan and Christodoulos, 1993; Ceperley, 1995, 1996; Nielaba, 1997; Assad and Evertz, 2008). Thus in this chapter we can by no means attempt an exhaustive coverage of this rapidly developing field. Instead we present a tutorial introduction to some basic aspects and then describe some simple applications.

8.2 FEYNMAN PATH INTEGRAL FORMULATION

8.2.1 Off-lattice problems: low temperature properties of crystals

We begin with the problem of evaluating thermal averages in the framework of quantum statistical mechanics. The expectation value for some quantum

mechanical operator $\hat{A}$ corresponding to the physical observable A, for a system of N quantum particles in a volume V, is given by

$$\langle \hat{A} \rangle = Z^{-1} \mathrm{Tr} \exp(-\mathcal{H}/k_\mathrm{B}T)\hat{A} = Z^{-1} \sum_n \langle n|\exp(-\mathcal{H}/k_\mathrm{B}T)\hat{\mathrm{A}}|n\rangle, \tag{8.1}$$

with

$$Z = \mathrm{Tr} \exp(-\mathcal{H}/k_\mathrm{B}T) = \sum_n \langle n|\exp(-\mathcal{H}/k_\mathrm{B}T)|n\rangle, \tag{8.2}$$

where $\mathcal{H}$ is the Hamiltonian, and the states $|n\rangle$ form a complete, orthonormal basis set. In general, the eigenvalues E_α of the Hamiltonian ($\mathcal{H}|\alpha\rangle = E_\alpha|\alpha\rangle$ with eigenstate $|\alpha\rangle$) are not known, and we wish to evaluate the traces in Eqns. (8.1) and (8.2) without attempting to diagonalize the Hamiltonian. This task is possible with the Feynman path integral approach (Feynman and Hibbs, 1965). The basic idea of this method can be explained for a single particle of mass m in a potential $V(x)$, for which the Hamiltonian (in position representation) reads

$$\mathcal{H} = \hat{E}_\mathrm{kin} + \hat{V} = -\frac{\hbar^2}{2m}\frac{d^2}{dx^2} + V(x), \tag{8.3}$$

and using the states $|x\rangle$ as a basis set the trace Z becomes

$$Z = \int dx \langle x|\exp(-\mathcal{H}/k_\mathrm{B}T)|x\rangle = \int dx \langle x|\exp[-(\hat{E}_\mathrm{kin} + \hat{V})/k_\mathrm{B}T]|x\rangle. \tag{8.4}$$

If $\hat{E}_\mathrm{kin}$ and $\hat{V}$ commuted, we could replace $\exp[-(\hat{E}_\mathrm{kin} + \hat{V})/k_\mathrm{B}T]$ by $\exp(-\hat{E}_\mathrm{kin}/k_\mathrm{B}T)\exp(-\hat{V}/k_\mathrm{B}T)$ and, by inserting the identity $\hat{1} = \int dx'|x'\rangle\langle x'|$, we would have solved the problem, since $\langle x'|\exp[-\hat{V}(x)/k_\mathrm{B}T]|x\rangle = \exp[-V(x)/k_\mathrm{B}T]\delta(x - x')$ and $\langle x|\exp[-\hat{E}_\mathrm{kin}/k_\mathrm{B}T]|x'\rangle$ amounts to dealing with the quantum mechanical propagator of a free particle. However, by neglecting the non-commutativity of $\hat{E}_\mathrm{kin}$ and $\hat{V}$, we reduce the problem back to the realm of classical statistical mechanics, all quantum effects would be lost.

A related recipe is provided by the exact Trotter product formula (Trotter, 1959; Suzuki, 1971) for two non-commuting operators $\hat{A}$ and $\hat{B}$:

$$\exp(\hat{A} + \hat{B}) \underset{P\to\infty}{\to} [\exp(\hat{A}/P)\exp(\hat{B}/P)]^P, \tag{8.5}$$

where P is an integer. In the specific case of a single particle moving in a potential, the Trotter formula becomes

$$\exp[-(\hat{E}_\mathrm{kin}+\hat{V})/k_\mathrm{B}T] = \lim_{P\to\infty} \{\exp(-\hat{E}_\mathrm{kin}/k_\mathrm{B}TP)\ \exp(-\hat{V}/k_\mathrm{B}TP)\}^P. \tag{8.6}$$

As a result, we can rewrite the partition function Z as follows

$$\begin{aligned} Z = \lim_{P\to\infty} \int dx_1 \int dx_2 \ldots \int dx_P \langle x_1|\exp(-\hat{E}_{\rm kin}/k_{\rm B}TP)\exp(-\hat{V}/k_{\rm B}TP)|x_2\rangle \\ \times\langle x_2|\exp(-\hat{E}_{\rm kin}/k_{\rm B}TP)\ \exp(-\hat{V}/k_{\rm B}TP)|x_3\rangle\langle x_3|\ldots|x_P\rangle \\ \times\langle x_P|\exp(-\hat{E}_{\rm kin}/k_{\rm B}TP)\ \exp(-\hat{V}/k_{\rm B}TP)|x_1\rangle. \end{aligned} \tag{8.7}$$

In practice, it will suffice to work with a large but finite P, and since the matrix elements can be worked out as follows:

$$\begin{aligned} &\langle x|\exp(-\hat{E}_{\rm kin}/k_{\rm B}TP)\ \exp(-\hat{V}/k_{\rm B}TP)|x'\rangle \\ &= \left(\frac{m k_{\rm B}TP}{2\pi\ \hbar^2}\right)^{1/2} \exp\left[-\frac{m k_{\rm B}TP}{2\ \hbar^2}(x-x')^2\right]\exp\left[-\frac{V(x)+V(x')}{2k_{\rm B}TP}\right], \end{aligned} \tag{8.8}$$

we obtain the following approximate result for the partition function:

$$\begin{aligned} Z \approx \left(\frac{m k_{\rm B}TP}{2\pi\ \hbar^2}\right)^{P/2} \int dx_1 \cdots dx_P \\ \times\exp\left\{-\frac{1}{k_{\rm B}T}\left[\frac{\kappa}{2}\sum_{s=1}^{P}(x_s - x_{s+1})^2 + \frac{1}{P}\sum_{s=1}^{P}V(x_s)\right]\right\}, \end{aligned} \tag{8.9}$$

where the boundary condition $x_{P+1} = x_1$ holds and the effective spring constant is

$$\kappa = mP(k_{\rm B}T)^2/\hbar^2. \tag{8.10}$$

Equation (8.9) is equivalent to the classical configurational partition function of P classical particles coupled with a harmonic potential $V(x)$, in a kind of 'ring polymer'. When one generalizes this to N particles interacting with a pair potential in d dimensions,

$$\mathcal{H} = \sum_{i=1}^{N}\left(-\frac{\hbar^2}{2m}\nabla_i^2\right) + \sum_{i<j} V(|\mathbf{r}_i - \mathbf{r}_j|), \tag{8.11}$$

one finds that the resulting 'melt' of cyclic polymers has somewhat unusual properties, since monomer–monomer interactions occur only if the 'Trotter index' is the same. Thus the partition function becomes ($\mathbf{r}_i^{(s)}$ is the coordinate of the ith particle in the sth slice of the imaginary time variable)

$$\begin{aligned} Z &= \left(\frac{m k_{\rm B}TP}{2\pi\ \hbar^2}\right)^{dNP/2} \int d\mathbf{r}_1^{(1)} \cdots \int d\mathbf{r}_N^{(P)} \\ &\quad\times\ \exp\left\{-\frac{1}{k_{\rm B}T}\left[\frac{\kappa}{2}\sum_{i=1}^{N}\sum_{s=1}^{P}\left(r_i^{(s)} - r_i^{(s+1)}\right)^2 + \frac{1}{P}\sum_{i<j}\sum_{s=1}^{P}V\left(\left|\mathbf{r}_i^{(s)} - \mathbf{r}_j^{(s)}\right|\right)\right]\right\} \\ &= \left(\frac{m k_{\rm B}T}{2\pi\ \hbar^2}\right)^{dNP/2} \int d\mathbf{r}_1^{(1)} \cdots \int d\mathbf{r}_N^{(P)} \exp\left\{-\mathcal{H}_{\rm eff}^{(P)}/k_{\rm B}T\right\}. \end{aligned} \tag{8.12}$$

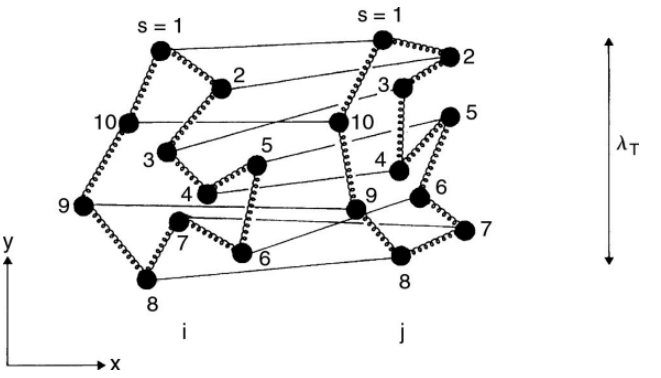

Fig. 8.1 Schematic representation of two interacting quantum particles i, j in two dimensions: each particle (i) is represented by a 'ring polymer' composed of $P = 10$ effective monomers $\mathrm{r}_i^{(s)}$, with $s = 1, \ldots, P$. Harmonic springs (of strength κ) only connect 'monomers' in the same 'polymer', while interatomic forces join different monomers with the same Trotter index s, indicated by the thin straight lines. In the absence of such interactions, the size of such a ring polymer coil would be given by the thermal de Broglie wavelength, $\lambda_T = h/\sqrt{2\pi m k_\mathrm{B} T}$, where h is Planck's constant.

This 'ring polymer' is shown schematically in Fig. 8.1. If the effect of the potential V could be neglected, we could simply conclude from the equipartition theorem (since Eqns. (8.9) and (8.12) can be viewed as a problem in classical statistical mechanics, this theorem applies), that the potential energy carried by each spring is $(d/2)k_\mathrm{B}T = (\kappa/2)\langle(\mathbf{r}_i^{(s)} - \mathbf{r}_i^{(s+1)})^2\rangle$, i.e. the typical interparticle mean-square displacement of two neighboring particles along the chain is $\ell^2 = \langle(\mathbf{r}_i^{(s)} - \mathbf{r}_i^{(s+1)})^2\rangle = dk_\mathrm{B}T/\kappa = \hbar^2 d/(mk_\mathrm{B}TP)$. Now the gyration radius of a ring polymer containing P monomers is $\langle R_g^2\rangle = \ell^2 P/12 = (d/12)(\hbar^2/mk_\mathrm{B}T)$. Thus we see that the diameter $2\sqrt{\langle R_g^2\rangle} = \hbar\sqrt{(d/3mk_\mathrm{B}T)}$ is of the same order as the thermal de Broglie wavelength $\lambda_T = h/\sqrt{2\pi m k_\mathrm{B} T}$ of a particle. This formalism brings out in a very direct fashion the fact that in quantum mechanics the uncertainty principle forbids the simultaneous precise specification of both momenta and positions of the particles; and for free particles, integrating out the momenta then leaves the particles delocalized in space in 'cells' of linear dimension λ_T. The advantage of the formalism written in Eqns. (8.9)–(8.12) is, of course, that it remains fully valid in the presence of the potential $V(|\mathbf{r}_i - \mathbf{r}_j|)$ – then the linear dimension of the delocalization no longer is simply given by λ_T, but depends on the potential V as well. This fact is well known for harmonic crystals, of course: the delocalization of an atom in a harmonic crystal can be expressed in terms of the harmonic oscillator groundstate wave functions, summed over all eigenfrequencies ω_q of the crystal. In other words, the mean-square displacement of an atom around the position in the ideal rigid lattice for $T - 0$ is $\langle\mathbf{r}_i^2\rangle = (1/2Nm)\sum_\mathrm{q}(\hbar\omega_\mathrm{q})^{-1}$. On the other hand, one knows that the harmonic approximation for crystals has many deficiencies, e.g. it does not describe thermal expansion. As an example, Fig. 8.2 compares the lattice constant $a(T)$ of orthorhombic solid polyethylene, as deduced from a PIMC calculation (Martonak *et al.*, 1998), with the corresponding classical results and with experiment (Dadobaev and Slutsker, 1981). Clearly the classical Monte

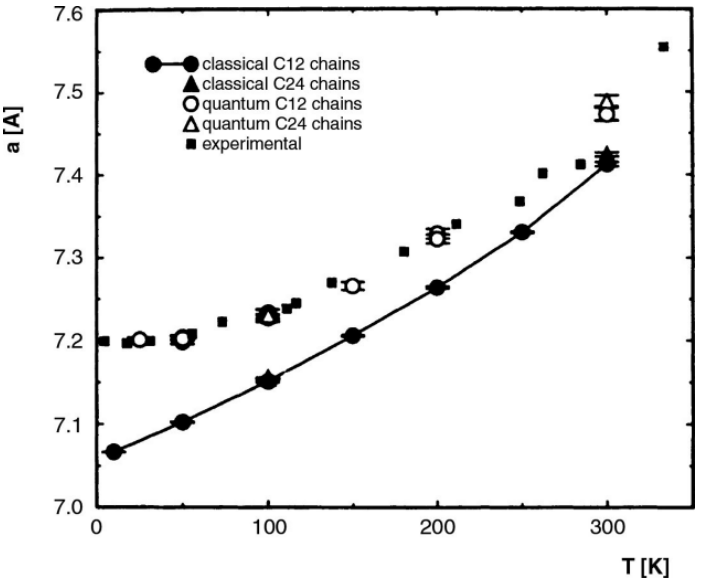

Fig. 8.2 Temperature dependence of the lattice constant for orthorhombic polyethylene. Results of a PIMC calculation are compared with the value for a classical system and with experiment. After Martonak *et al.* (1998).

Carlo result underestimates $a(T)$ systematically at all temperatures from $T = 0$ K to room temperature, and yields a constant thermal expansion coefficient $\alpha = a^{-1}da/dT$ as $T \to 0$, in contrast to the result $a(T \to 0) \to 0$ required by the third law of thermodynamics. The PIMC results are clearly in accord with this law, as they should be, and even reproduce the experimental data perfectly, although such good agreement is to some extent fortuitous in view of the uncertainties about the potentials to be used for this polymer.

Now it is well known that one can go somewhat beyond the harmonic approximation in the theory of the dynamics of crystal lattices, e.g. by taking entropy into account via the quasi-harmonic approximation that uses a quadratic expansion around the minimum of the free energy rather than the potential energy, as is done in the standard harmonic approximation. In fact, such a quasi-harmonic lattice dynamics study of orthorhombic polyethylene has also been carried out (Rutledge *et al.*, 1998), and the comparison with the PIMC results shows that the two approaches do agree very nicely at temperatures below room temperature. However, only the PIMC approach in this example is reliable at room temperature and above, up to the melting temperature, where quantum effects gradually die out and the system starts to behave classically. Also, the PIMC method yields information on local properties involving more than two atoms in a very convenient way, e.g. the mean-square fluctuation of the bond angle θ_{CCC} between two successive carbon-carbon bonds along the backbone of the $C_n\,H_{2n+2}$ chain (Fig. 8.3), which would be rather cumbersome to obtain by lattice dynamics methods. While according to classical statistical mechanics such a bond angle fluctuation vanishes as $T \to 0$, i.e. $\sqrt{\langle(\delta\theta_{\mathrm{CCC}})^2\rangle} \propto \sqrt{T}$, so that in the groundstate ($T = 0$) a perfectly rigid zig-zag structure (Fig. 6.17) remains, this is not true when one considers quantum mechanics and bond angles then fluctuate by around 3 degrees. Even

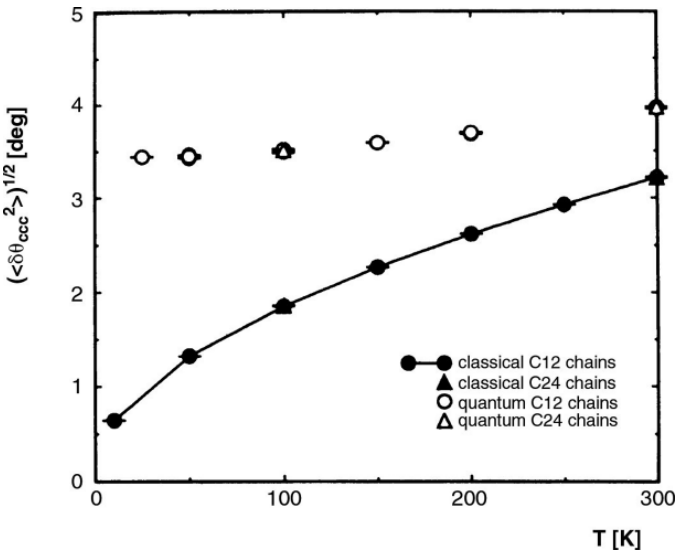

Fig. 8.3 Temperature dependence of the average fluctuation $\sqrt{\langle(\delta\theta_{CCC})^2\rangle}$ of the C – C – C bond angle, according to the classical Monte Carlo calculation (full dots) and according to PIMC simulations (open symbols), for two choices of chain length n ($n = 12$ and $n = 24$, respectively). From Martonak *et al.* (1998).

at room temperature the classical calculation underestimates this fluctuation still by about 20%.

Now one point which deserves comment is the proper choice of the Trotter dimension P. According to Eqn. (8.6), the method is only exact in the limit $P \to \infty$. This presents a serious problem as does the extrapolation to the thermodynamic limit, $N \to \infty$. Just as one often wishes to work with as small N as possible, for the sake of an economical use of computer resources, one also does not wish to choose P unnecessarily large. However, since the distance between points along the ring polymer in Fig. 8.1 scales as $\ell^2 \propto (TP)^{-1}$ as argued above, and we have to keep this distance small in comparison to the length scales characterizing the potential, it is obvious that the product TP must be kept fixed so that ℓ is fixed. As the temperature T is lowered, P must be chosen to be larger. Noting that for operators $\hat{A}$, $\hat{B}$ whose commutator is a complex number c, i.e. $[\hat{A}, \hat{B}] = c$, we have the formula

$$\exp[\hat{A} + \hat{B}] = \exp(\hat{A}) \exp(\hat{B}) \exp\left(-\tfrac{1}{2}[\hat{A}, \hat{B}]\right), \tag{8.13}$$

we conclude that for large P the error in replacing $\exp[-(\hat{E}_{\text{kin}} + \hat{V})/Pk_{\text{B}}T]$ by $\exp[-(\hat{E}_{\text{kin}}/Pk_{\text{B}}T)]\exp[-(\hat{V}/Pk_{\text{B}}T)]$ is of order $1/P^2$. This observation suggests that simulations should be tried for several values of P and the data extrapolated vs. $1/P^2$. In favorable cases the asymptotic region of this 'Trotter scaling' is indeed reached, as Fig. 8.4 demonstrates. This figure also shows that PIMC is able to identify typical quantum mechanical effects such as 'isotope effects': the two isotopes ^{20}Ne and ^{22}Ne of the Lennard–Jones system neon differ only by their mass, and in classical statistical mechanics there would be no difference in static properties whatsoever. However, as Fig. 8.4 shows, there is a clear distinction between the lattice constants of the two isotopes, and the difference observed in the simulation in fact is rather close to the value found in the experiment (Batchelder *et al.*, 1968). The examples shown

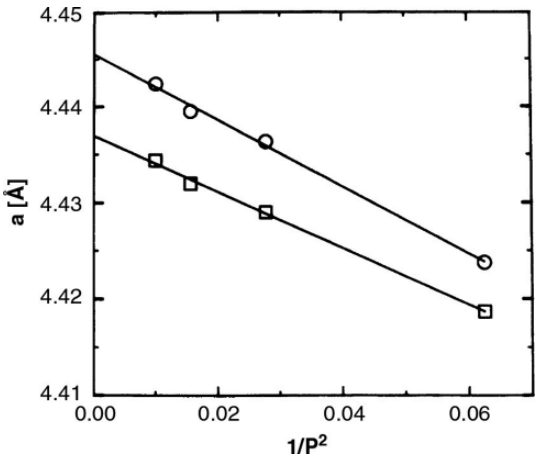

Fig. 8.4 Trotter scaling plot for the lattice parameter a of solid neon. The upper curve corresponds to ^{20}Ne at $T = 16$ K. From Müser *et al.* (1995).

should not leave the reader in a too optimistic mood, however, since there are also examples in the literature where even Trotter numbers as large as $P = 100$ are insufficient to reach this Trotter scaling limit. Indeed, not all quantities are equally well suited for such an extrapolation. Particularly cumbersome, for instance, is the specific heat for an insulating crystal which is expected to vary like $C \propto T^d$ at low temperatures in d dimensions (Debye law). However, the theory of lattice dynamics shows that this behavior results from long wavelength acoustic phonons, with frequency $\omega_q = c_s|\mathbf{q}|$, where c_s is the speed of sound and $\mathbf{q}$ their wavevector. In a finite cubic crystal of size $L \times L \times L$ with periodic boundary conditions the smallest $|\mathbf{q}|$ that fits is of order $2\pi/L$, and hence the phonon spectrum is cut off at a minimum frequency $\omega_{\min} \propto c_s/L$. Due to this gap in the phonon spectrum at low enough temperatures ($k_B T < \hbar\omega_{\min}$) the specific heat does not comply with the Debye law, but rather behaves as $C \propto \exp(-\hbar\omega_{\min}/k_B T)$. In order to deal with such problems, Müser *et al.* (1995) proposed a combined Trotter and finite size scaling. In this context, we also emphasize that the specific heat *cannot* be found from computing fluctuations of the effective Hamiltonian $H_{\text{eff}}^{(P)}$, Eqn. (8.9), $\langle \mathcal{H}_{\text{eff}}^{(P)2} \rangle - \langle \mathcal{H}_{\text{eff}}^{(P)} \rangle^2$. The reason is that the spring constant κ, Eqn. (8.10), is temperature-dependent, and this fact invalidates the standard derivation of the fluctuation formula. For suitable estimators of the specific heat and other response functions in Monte Carlo calculations we refer to the more specialized literature quoted in Section 8.1.

Problem 8.1 Consider a single particle in a harmonic potential well with characteristic frequency of $\omega = (k/m)^{1/2}$. Perform a path integral Monte Carlo simulation for $P = 1$, $P = 2$, and $P = 8$ at an inverse temperature of $\beta = 2.5$. Carry out multiple runs for 10 000 MC steps and determine statistical error bars. Repeat the calculation for runs of 10^6 Monte Carlo steps. Compare the results and comment.

8.2.2 Bose statistics and superfluidity

We now mention another important problem: in making the jump from the one-particle problem, Eqn. (8.6), to the N-particle problem, Eqn. (8.12), we have disregarded the statistics of the particles (Bose–Einstein vs. Fermi–Dirac statistics) and have treated them as distinguishable. For crystals of not too light atoms, this approximation is acceptable, but it fails for quantum crystals such as solid ^{3}He and ^{4}He, as well as for quantum fluids (Ceperley, 1995). For Bose systems, only totally symmetric eigenfunctions contribute to the density matrix, and hence if we write symbolically $\mathbf{R} = (\mathbf{r}_1, \mathbf{r}_2, \ldots, \mathbf{r}_N)$ and we define a permutation of particle labels by $\hat{P}\mathbf{R}$, where $\hat{P}$ is the permutation operator, we have for any eigenfunction $\phi_\alpha(\mathbf{R})$

$$\hat{P}\phi_\alpha(\mathbf{R}) = \frac{1}{N!}\sum_P \phi(\hat{P}\mathbf{R}), \tag{8.14}$$

where the sum is over all permutations of particle labels. The partition function for a Bose system therefore takes the form (Ceperley, 1995)

$$Z_B = \left(\frac{m k_\mathrm{B} TP}{2\pi\ \hbar^2}\right)^{dNP/2} \frac{1}{N!}\int d\mathbf{r}_1^{(1)} \cdots \int d\mathbf{r}_N^{(P)} \exp\left\{-\mathcal{H}_{\mathrm{eff}}^{(P)}/k_\mathrm{B}T\right\}, \tag{8.15}$$

where now the boundary condition is not $\mathbf{r}_i^{(\mathrm{P}+1)} = \mathbf{r}_i^{(1)}$ as in Eqn. (8.10), but rather $\hat{P}\mathbf{R}^{(P+1)} = \mathbf{R}^{(1)}$. This means that paths are allowed to close on any permutation of their starting positions, and contributions from all $N!$ closures are contained in the partition function. At high temperatures the identity permutation yields the dominating contribution, while at zero temperature all permutations have equal weight. In the classical isomorphic system, this means that 'crosslinks' form and open up again in the system of ring polymers. (Of course, such behavior should not be confused with the actual chemical kinetics of polymerization and crosslinking processes of real polymers.) A two-atom system with P effective monomers can be in two possible permutation states: either two separate ring polymers, each with P springs (as shown in Fig. 8.1), or one larger ring polymer with $2P$ springs.

At this point, it is illuminating to ask what superfluidity (such as actually occurs in ^{4}He) implies in this formalism (Feynman, 1953): a macroscopic polymer is formed which involves on the order of N atoms and stretches over the entire system. From Fig. 8.1, it is clear that this 'crosslinking' among ring polymers can set in only when the linear dimension of a ring polymer coil becomes of the same order as the 'interpolymer spacing': in this way one can get an order of magnitude estimate of the superfluid transition temperature T_λ, by putting the thermal de Broglie wavelength $\lambda_\mathrm{T} = h\sqrt{2\pi m k_\mathrm{B} T}$ equal to the 'interpolymer spacing', $\rho^{-1/\mathrm{d}}$, where ρ is the density of the d-dimensional system. The 'degeneracy temperature' T_D found from $\lambda_\mathrm{T} = \rho^{-1/\mathrm{d}}$, i.e. $T_\mathrm{D} = \rho^{2/\mathrm{d}}h^2/(2\pi k_\mathrm{B} m)$, sets the temperature scale on which important quantum effects occur.

In practice, use of Eqns. (8.12) and (8.15) would not work for the study of superfluidity in ^{4}He – although the formalism is exact in principle, values of P which are unreasonably large would be required for satisfactory results. An alternative approach is to use what is called an 'improved action' rather than the 'primitive action' $\mathcal{H}_{\text{eff}}/k_{\text{B}}T$ given in Eqn. (8.12). However, we shall not go into any detail here but rather refer the reader to the original literature (e.g. Ceperley, 1995).

Although 'standard' methods have worked well for small systems of weakly interacting bosons in the continuum (see, e.g., Nho and Landau (2004) for systems with up to 216 hard core bosons), a new 'worm algorithm' has permitted the extension to much larger systems. The worm algorithm developed by Boninsegni *et al.* (2006a, b) permits the simulation of much larger systems. This method operates in an extended ensemble space and includes both closed, world-line configurations as well as configurations that contain an open world-line, or 'worm'. Possible moves include closing an open or removing an existing open world-line, or, alternatively, creating a new open world-line or opening an existing closed one. The worm algorithm overcomes the exponential inefficiency with which long permutation cycles are sampled and permits a much closer approach to the thermodynamic limit. Of course, in most cases some sort of finite size scaling method is ultimately used to analyze the data. Boninsegni *et al.* (2006a, b) performed simulations of up to 2048 ^{4}He atoms and found a crossing of the winding number curves at $T_{\text{c}} = 2.193(6)$ K, which is very close to the experimental value of 2.177 K.

The treatment of fermions is even more cumbersome. The straightforward application of PIMC to fermions means that odd permutations subtract from the sum: this is an expression of the 'minus sign problem' that hampers all Monte Carlo work on fermions. In fact, PIMC for fermions in practice requires additional approximations and is less useful than for bosons or for 'Boltzmannons' (i.e. cases where the statistics of the particles can be neglected altogether, as for the behavior of slightly anharmonic crystals formed from rather heavy particles, as discussed in the beginning of this section). We refer the reader to Ceperley (1996) for a review of this problem.

8.2.3 Path integral formulation for rotational degrees of freedom

So far the discussion has tacitly assumed point-like particles and the kinetic energy operator $\hat{E}_{\text{kin}}$ (Eqns. (8.3) and (8.4)) was meant to describe their translational motion; however, rather than dealing with the effects due to non-commutativity of position operator ($\mathbf{x}$) and momentum operator ($\mathbf{p}$), $\left[\hat{x}_\alpha, \hat{p}_\beta\right] = i\hbar\delta_{\alpha\beta}$, we may also consider effects due to the non-commutativity of the components of the angular momentum operator, $\hat{L}_\alpha$. Such effects are encountered, for example, in the description of molecular crystals, where the essential degrees of freedom that one wishes to consider are the polar angles (θ_i, φ_i) describing the orientation of a molecule (Müser, 1996). Here we discuss

only the simple special case where the rotation of the molecules is confined to a particular plane. For example, in monolayers of N_2 adsorbed on graphite in the commensurate $\sqrt{3} \times \sqrt{3}$ structure (Marx and Wiechert, 1996), one can ignore both the translational degree of freedom of the N_2 molecules and the out-of-plane rotation, i.e. the angle $\theta_i = \pi/2$ is not fluctuating, the only degree of freedom that one wishes to consider is the angle φ_i describing the orientation in the xy-plane, parallel to the graphite substrate. The Hamiltonian hence is (I is the moment of inertia of the molecules, and $\hat{V}$ the intermolecular potential)

$$\mathcal{H} = \sum_{j=1}^{N} \frac{\hat{L}_{jZ}^2}{2I} + \sum_{i \neq j} \hat{V}(\varphi_i, \varphi_j), \tag{8.16}$$

since the commutation relation $[\hat{L}_{jZ}^2, \hat{\varphi}_i] = -i\hbar\delta_{j,i}$ is analogous to that of momentum and position operator, one might think that the generalization of the PIMC formalism (Eqns. (8.9)–(8.12)) to the present case is trivial, but this is not true due to the rotation symmetry $\varphi_j = \varphi_j + n_j 2\pi$, with n_j integer: if we write the partition function as path integral we obtain (Marx and Nielaba, 1992)

$$Z = \left(\frac{Ik_{\mathrm{B}}TP}{2\pi\,\hbar^2}\right)^{NP/2} \prod_{j=1}^{N} \left\{ \sum_{n_j=-\infty}^{+\infty} \int_0^{2\pi} d\varphi_i^{(1)} \prod_{s=2}^{P} \int_{-\infty}^{+\infty} d\varphi_j^{(s)} \right\} \exp\left[-H_{\mathrm{eff}}^{(P)} / k_{\mathrm{B}}T\right], \tag{8.17}$$

with

$$\mathcal{H}_{\mathrm{eff}}^{(P)} = \sum_{s=1}^{P} \left\{ \sum_{j=1}^{N} \frac{IPk_{\mathrm{B}}^2T^2}{2\hbar^2} \left[\varphi_j^{(s)} - \varphi_j^{(s+1)} + 2\pi n_j \delta_{S,P}\right]^2 + \sum_{\langle i.j \rangle}^{N} \frac{1}{P} V\left(\varphi_i^{(s)}, \varphi_j^{(s)}\right) \right\}. \tag{8.18}$$

Thus each quantum mechanical rotational degree of freedom is represented in this path integral representation by P classical rotators, which form closed loops and interact via harmonic type interactions. In addition there is the potential $V(\varphi_i^{(s)}, \varphi_j^{(s)})$ denoting the pair potential evaluated separately for the configuration at each imaginary-time slice $s = 1, \ldots, P$. However, in contrast to path integrals for translational degrees of freedom, the loops need not be closed using periodic boundary conditions, but only modulo 2π: the classical angles are not confined to $[0, 2\pi]$ but are allowed on the whole interval $[-\infty, +\infty]$. The resulting mismatch n_j is called the 'winding number' of the jth path and Eqns. (8.17) and (8.18) yield the 'winding number representation' of the partition function. Only the Boltzmann-weighted summation over all possible winding numbers in addition to the integration over all paths having a certain winding number yields the correct quantum partition function in the Trotter limit $P \to \infty$. Thus the Monte Carlo algorithm has to include both moves that

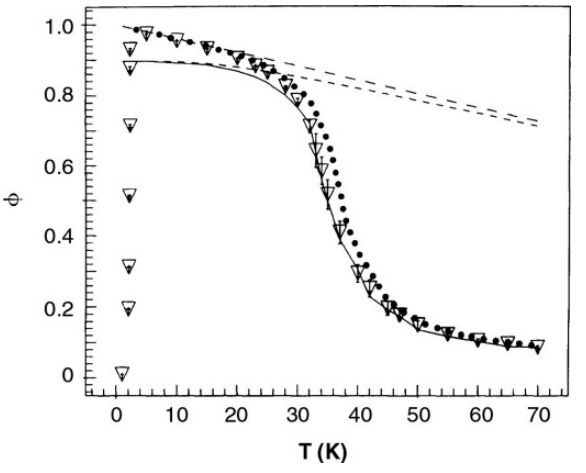

Fig. 8.5 Herringbone structure order parameter for a model of N_2 plotted vs. temperature. Quantum simulation, full line; classical simulation, dotted line; quasi-harmonic theory, dashed line; Feynman–Hibbs quasi-classical approximation, triangles. From Marx *et al.* (1993).

update the angular degrees of freedom $\{\varphi_j^{(s)} \to \varphi_j^{(s)'}\}$ and moves that attempt to change the winding number, $n_j \to n_j'$.

As an example of problems that can be tackled with such techniques, Fig. 8.5 shows the order parameter ϕ of a model for N_2 on graphite. This order parameter describes the ordering of the so-called herringbone structure, and is calculated from the three order parameter components ϕ_α as $\phi = \langle[\sum_{\alpha=1}^{3}\phi_\alpha^2]^{1/2}\rangle$, with

$$\phi_\alpha = \frac{1}{N}\frac{1}{P}\sum_{j=1}^{N}\sum_{s=1}^{P}\sin\left(2\varphi_j^{(s)} - 2\eta_\alpha\right)\exp[\mathbf{Q}_\alpha \cdot \mathbf{R}_j], \tag{8.19}$$

where $\mathbf{R}_j$ is the center of mass position of the jth molecule, the $\mathbf{Q}_\alpha$ are wavevectors characteristic for the ordering $\{\mathbf{Q}_1 = \pi(0, 2/\sqrt{3}); \mathbf{Q}_2 = \pi(-1, -1/\sqrt{3}); \mathbf{Q}_3 = \pi(1, -1/\sqrt{3})\}$ and the phases η_i are $\eta_1 = 0$, $\eta_2 = 2\pi/3$, and $\eta_3 = 4\pi/3$. Using $N = 900$ rotators, even for $T > T_c$ we have the characteristic 'finite size tail' in both the classical and in the quantum calculations. The critical temperature T_c of the classical model has been estimated as 38 K. While at high temperatures classical and quantum calculations merge, near T_c the quantum mechanical result deviates from the classical one, since in this model the quantum fluctuations reduce T_c by about 10%. Furthermore, one can infer that the quantum system does not reach the maximum herringbone ordering ($\phi = 1$) even at $T \to 0$: the quantum librations depress the saturation value by 10%. In Fig. 8.5 the order parameter, as obtained from the full quantum simulation, is compared with two approximate treatments valid at low and high temperatures: quasi-harmonic theory can account for the data for $T > 10$ K but fails completely near the phase transition; the Feynman–Hibbs quasi-classical approximation (based on a quadratic expansion of the effective Hamiltonian around the classical path) works very well at high temperatures, but it starts to deviate from the correct curve just below T_c and completely breaks down as $T \to 0$. We see that all these approximate treatments are

uncontrolled, their accuracy can only be judged a posteriori; only the PIMC simulation yields correct results over the whole temperature range from the classical to the quantum regime.

8.3 LATTICE PROBLEMS

8.3.1 The Ising model in a transverse field

The general idea that one follows to develop a useful path integral formulation of quantum models on lattices is again the strategy to decompose the Hamiltonian $\mathcal{H}$ of the interacting many-body system into sums of operators that can be diagonalized separately. The Trotter formula can be then used in analogy with Eqn. (8.6), for $\mathcal{H} = \mathcal{H}_1 + \mathcal{H}_2$ (Trotter, 1959; Suzuki, 1971)

$$\exp[-(\mathcal{H}_1 + \mathcal{H}_2)/k_\mathrm{B}T] = \lim_{P\to\infty} \{\exp(-\mathcal{H}_1/k_\mathrm{B}TP)\exp(-\mathcal{H}_2/k_\mathrm{B}TP)\}^P. \tag{8.20}$$

Note that there is no general recipe for how this division of $\mathcal{H}$ into parts should be done – what is appropriate depends on the nature of the model. Therefore, there are many different variants of calculations possible for certain models, and generalizations of Eqn. (8.20), where the error is not of order $1/P^2$ but of even higher inverse order in P, have also been considered (Suzuki, 1976a, 1976b, 1992).

To illustrate the general principles of the approach we consider a model for which all calculations can be carried out exactly, namely the one-dimensional Ising model in a transverse field. We take (de Raedt and Lagendijk, 1985)

$$\mathcal{H}_1 = -\mathcal{J}\sum_{i=1}^{N} \hat{\sigma}_i^z \hat{\sigma}_{i+1}^z, \qquad \mathcal{H}_2 = -H_\perp \sum_{i=1}^{N} \hat{\sigma}_i^x, \tag{8.21}$$

where $\hat{\sigma}_i^\alpha (\alpha = x, y, z)$ denote the Pauli spin matrices at site i. We assume periodic boundary conditions, $\hat{\sigma}_{N+1}^\alpha = \hat{\sigma}_1^\alpha$. For the representation we choose the eigenstates of $\hat{\sigma}^z$ and label them by Ising spin variables, $S = \pm 1$, i.e. $\hat{\sigma}^z|S\rangle = S|S\rangle$. Of course, $\mathcal{H}_1$ is diagonal in this representation. We then find for the Pth approximant to the partition function

$$\begin{aligned} Z_p &= \mathrm{Tr}[\exp(-\mathcal{H}_1/k_\mathrm{B}TP)\exp(-\mathcal{H}_2/k_\mathrm{B}TP)]^P \\ &= \sum_{\{S_i^{(k)}\}} \prod_{k=1}^{P}\prod_{i=1}^{N} \exp\left[\frac{\mathcal{J}}{k_\mathrm{B}TP} S_i^{(k)} S_{i+1}^{(k)}\right] \left\langle S_i^{(k)} \left| \exp\left(\frac{H_\perp \hat{\sigma}_i^x}{k_\mathrm{B}TP}\right) \right| S_i^{(k+1)} \right\rangle. \end{aligned} \tag{8.22}$$

In this trace we have to take periodic boundary conditions in the imaginary time direction as well, $S_i^{(k)} = S_i^{(k+P)}$. Now the matrix element in Eqn. (8.22) is evaluated as follows:

$$\langle S|\exp(a\hat{\sigma}^x)|S'\rangle = \left(\tfrac{1}{2}\sinh\ 2a\right)^{1/2} \exp\left(\tfrac{1}{2}\ln\coth a\right) SS'. \tag{8.23}$$

Substituting Eqn. (8.23) in Eqn. (8.22), we see that Z_p looks like the partition function of an anisotropic two-dimensional Ising model,

$$Z_p = C_p \sum_{\{S_i^{(k)}\}} \exp\left[\sum_{k=1}^{P}\sum_{i=1}^{N}\left(K_p S_i^{(k)} S_i^{(k+1)} + \frac{\mathcal{J}}{k_B TP} S_i^{(k)} S_{i+1}^{(k)}\right)\right], \tag{8.24}$$

with

$$C_p = \left[\tfrac{1}{2}\sinh\left(2H_\perp / k_B TP\right)\right]^{PN/2}, \quad K_p = \tfrac{1}{2}\ln\coth(H_\perp / k_B TP). \tag{8.25}$$

At this point we can use the rigorous solution of the finite two-dimensional Ising model (Onsager, 1944). Thus the one-dimensional quantum problem could be mapped onto an (anisotropic) two-dimensional classical problem, and this mapping extends to higher dimensions, as well. However, it is important to note that the couplings depend on the linear dimension P in the 'Trotter direction' and in this direction they also are temperature dependent (analogous to the spring constant κ in the polymer formalism derived above).

8.3.2 Anisotropic Heisenberg chain

A more complex and more illuminating application of the Trotter formula to a simple lattice model is to the spin-$\frac{1}{2}$ anisotropic Heisenberg chain,

$$\mathcal{H} = -\sum_i \left(\mathcal{J}_x \hat{S}_i^x \hat{S}_{i+1}^x + \mathcal{J}_y \hat{S}_i^y \hat{S}_{i+1}^y + \mathcal{J}_z \hat{S}_i^z \hat{S}_{i+1}^z\right). \tag{8.26}$$

For $\mathcal{J}_x = \mathcal{J}_y = \mathcal{J}_z$ this model is merely a simple quantum Heisenberg chain, and for $\mathcal{J}_x = \mathcal{J}_y$ and $\mathcal{J}_z = 0$ it becomes the quantum XY-chain. There are now several different ways in which the quantum Hamiltonian may be split up. The procedure first suggested by Suzuki (1976b) and Barma and Shastry (1978) was to divide the Hamiltonian by spin component, i.e.

$$\mathcal{H} = \mathcal{H}_0 + V_A + V_B, \tag{8.27a}$$

where

$$\mathcal{H}_0 = -\sum_{i=1}^{N} \mathcal{J}_z \hat{S}_i^z \hat{S}_{i+1}^z, \tag{8.27b}$$

$$V_A = \sum_{i \text{ odd}} V_i, \tag{8.27c}$$

$$V_B = \sum_{i \text{ even}} V_i, \tag{8.27d}$$

$$V_i = -\left(\mathcal{J}_x \hat{S}_i^x \hat{S}_{i+1}^x + \mathcal{J}_y \hat{S}_i^y \hat{S}_{i+1}^y\right). \tag{8.27e}$$

Applying Trotter's formula to the partition function we obtain

$$Z = \lim_{P\to\infty} Z^{(P)} \tag{8.28}$$

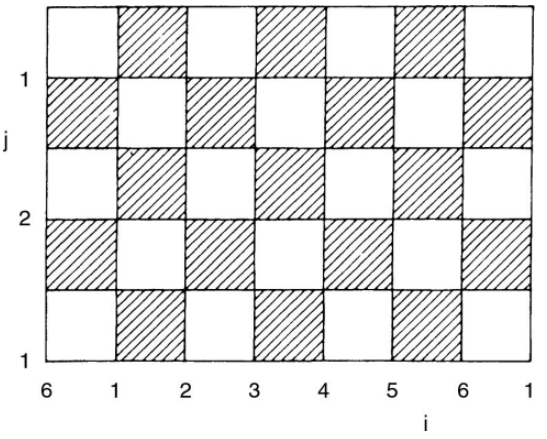

Fig. 8.6 Schematic view of the lattice produced by the Trotter–Suzuki transformation for the anisotropic Heisenberg chain. Two-spin interactions remain between nearest neighbors in the real space (horizontal) direction. The shaded squares represent four-spin couplings.

with

$$Z^{(P)} = \mathrm{Tr}\left(e^{-\beta\mathcal{H}_0/2P} e^{-\beta V_A/P} e^{-\beta\mathcal{H}_0/2P} e^{-\beta V_B/P}\right)^P, \tag{8.29}$$

where the limit $P \to \infty$ and the trace have been interchanged. Introducing $2P$ complete sets of eigenstates of $\mathcal{H}_0$ (the Ising part) so that there is one complete set between each exponential we obtain

$$Z^{(P)} = \sum_{\alpha_1\alpha_2\ldots\alpha_{2P}} \exp\left(\frac{-\beta}{2P}\sum_{r=1}^{2P}\mathcal{H}_{0r} - \beta\sum_{i\in A}\sum_{r=1}^{2P} h\,(i,r) - \beta\sum_{i\in B}\sum_{r=1}^{2P} h\,(i,r)\right) \tag{8.30}$$

where

$$e^{-\beta h(i,r)} = \left\langle S_{ir}\, S_{(i+1)r} \middle| e^{-\beta V_i/P} \middle| S_{i(r+1)} S_{(i+1)(r+1)} \right\rangle \tag{8.31}$$

and $S_{ir} = \pm 1/2$. Equation (8.30) can be interpreted as describing an $N \times 2P$ lattice with periodic boundary conditions and with two-spin interactions in the real space direction and temperature-dependent four-spin coupling on alternating elementary plaquettes, which couple neighboring sites in both real space and the Trotter direction, as shown in Fig. 8.6. Evaluation of the matrix elements in Eqn. (8.31) shows that only those plaquettes which have an even number of spins in each direction have non-zero weight, and these are enumerated in Fig. 8.7. (This result means that the classical model which results from the general, anisotropic Heisenberg chain is equivalent to an 8-vertex model; moreover, if $\mathcal{J}_x = \mathcal{J}_y$ it reduces further to a 6-vertex model.) Only those spin-flips which overturn an even number of spins are allowed, to insure that the trial state has non-zero weight, and the simplest possible such moves are either overturning all spins along a vertical line in the Trotter direction or those spins around a 'local' loop as shown in Fig. 8.8. We note further that if $\mathcal{J}_x = \mathcal{J}_y$ all allowed extensive flips change the magnetization of the system, whereas the local flips do not. There is one additional complication that needs to be mentioned: because of the temperature dependent interactions, the usual measures of the thermal properties are no longer corrrect. Thus, for example,

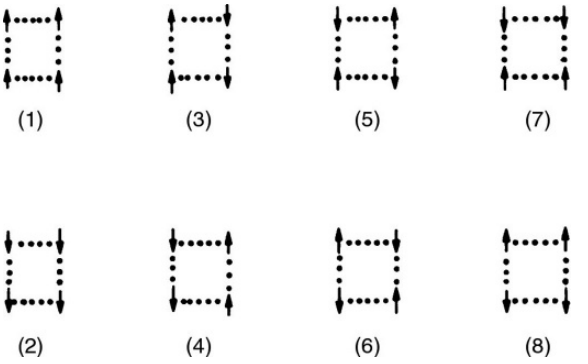

Fig. 8.7 The eight spin plaquettes with non-zero weight corresponding to the shaded squares in Fig. 8.6.

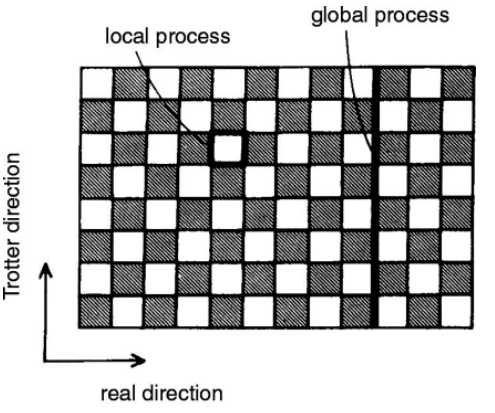

Fig. 8.8 Allowed spin-flip patterns (bold lines) for the lattice shown in Fig. 8.6.

the Pth approximant to the thermal average of the internal energy $E^{(P)}$ is

$$E^{(P)} = -\frac{\partial}{\partial\beta}\ln Z^{(P)}$$
$$= \frac{1}{Z^{(P)}}\sum_j F_j^{(P)} \exp\left(-\beta E_j^{(P)}\right), \tag{8.32}$$

where the sum is over all states and the 'energy function' F_j is now non-trivial. Similarly the calculation of the specific heat has an explicit contribution from the temperature dependence of the energy levels. Results for the antiferromagnetic Heisenberg chain, shown in Fig. 8.9, clearly indicate how the result for a fixed value of P approximates the quantum result only down to some temperature below which the data quickly descend to the classical value.

This procedure has been vectorized by Okabe and Kikuchi (1986) who assigned a plaquette number to each four-spin plaquette and noted that a simple XOR operation could be used to effect the spin plaquette flips. When this process was vectorized in an optimal fashion a speed of 34 million spin-flip trials per second could be achieved, a very impressive performance for the computers of that time.

Before we leave this section we wish to return to the question of how the Hamiltonian should be divided up before applying the Trotter transformation.

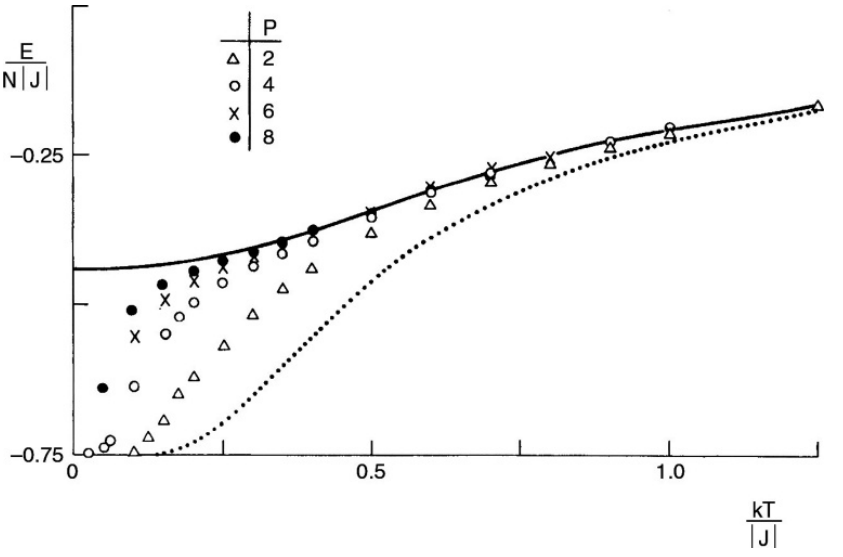

Fig. 8.9 Internal energy for the $S = \frac{1}{2}$ antiferromagnetic Heisenberg model. The solid line is the calculation of Bonner and Fisher (1964) and the dotted line is the exact $P = 1$ result from Suzuki (1966). From Cullen and Landau (1983).

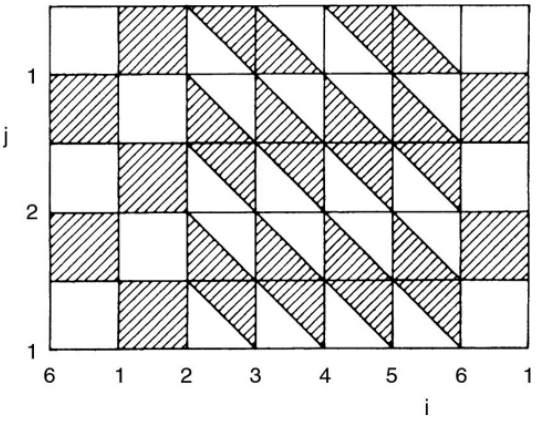

Fig. 8.10 Lattice produced by the alternate decomposition, given in Eqns. (8.33) for the $S = 1/2$ antiferromagnetic Heisenberg model.

An alternative to the decomposition used in the above discussion would have been to divide the system into two sets of non-interacting dimers, i.e.

$$\mathcal{H} = \mathcal{H}_1 + \mathcal{H}_2, \tag{8.33a}$$

where

$$\mathcal{H}_1 = -\sum_{i \in \text{odd}} \left(\mathcal{J}_x \hat{S}_i^x \hat{S}_{i+1}^x + \mathcal{J}_y \hat{S}_i^y \hat{S}_{i+1}^y + \mathcal{J}_z \hat{S}_i^z \hat{S}_{i+1}^z\right), \tag{8.33b}$$

$$\mathcal{H}_2 = -\sum_{i \in \text{even}} \left(\mathcal{J}_x \hat{S}_i^x \hat{S}_{i+1}^x + \mathcal{J}_y \hat{S}_i^y \hat{S}_{i+1}^y + \mathcal{J}_z \hat{S}_i^z \hat{S}_{i+1}^z\right). \tag{8.33c}$$

When the same process is repeated for this decomposition an $N \times 2P$ lattice is generated but the four-spin interactions have a different geometrical connectivity, as is shown in Fig. 8.10. In general then some thought needs to be given as to the best possible decomposition since there may be a number of different

possibilities which present themselves. This approach can be readily extended to higher dimensions and, in general, a d-dimensional quantum spin lattice will be transformed into a $(d+1)$-dimensional lattice with both two-spin couplings in the real space directions and four-spin interactions which connect different 'rows' in the Trotter direction.

8.3.3 Fermions on a lattice

The one-dimensional spin models considered in the previous section provide the opportunity to use the Trotter–Suzuki decomposition to help us understand concepts, to check the convergence as $P \to \infty$ and to test various refinements. New, non-trivial problems quickly arise when considering other relatively simple models such as spinless fermions in one dimension, where the Hamiltonian $\mathcal{H} = \mathcal{H}_1 + \mathcal{H}_2$ is written as

$$\mathcal{H} = -t \sum_{i=1}^{N} \left(\hat{c}_i^+ \hat{c}_{i+1} + \hat{c}_{i+1}^+ \hat{c}_i \right) + v_1 \sum_{i=1}^{N} \hat{n}_i \hat{n}_{i+1}. \tag{8.34}$$

The fermion operator $\hat{c}_i^+(\hat{c}_i)$ creates (annihilates) a particle at site i, and $\hat{n}_i \equiv \hat{c}_i^+ \hat{c}_i$ is the particle number operator, $\mathcal{N} = \sum_{i=1}^{N} n_i$ being the total number of particles ($\rho = \mathcal{N}/N$ then is the particle density). The hopping energy t is chosen to be unity, having the strength v_1 of the nearest neighbor interaction as a non-trivial energy scale in the model.

One of the standard tricks for dealing with quantum problems is to make use of clever transformations that make the problem more tractable. In the present situation, we first use Pauli matrices $\hat{\sigma}_i^{\alpha} (\alpha = x, y, z)$ to define spin-raising and spin-lowering operators by $\hat{\sigma}_\ell^+ = (\hat{\sigma}_\ell^x + i\hat{\sigma}_\ell^y)/2$ and $\hat{\sigma}_\ell^- = (\hat{\sigma}_\ell^x - i\hat{\sigma}_\ell^y)/2$, respectively, and express the $\hat{c}_\ell^+, \hat{c}_\ell$ in terms of the $\hat{\sigma}_\ell$ operators by a Jordan–Wigner transformation, which has a non-local character

$$\hat{c}_\ell^+ = \hat{\sigma}_\ell^+ \exp\left[\frac{i\pi}{2} \sum_{p=1}^{\ell-1} \left(1 + \hat{\sigma}_p^z\right) \right], \qquad \hat{c}_\ell = \hat{\sigma}_\ell^- \exp\left[-\frac{i\pi}{2} \sum_{p=1}^{\ell-1} \left(1 + \hat{\sigma}_p^z\right) \right]. \tag{8.35}$$

With this transformation the spinless fermion model, Eqn. (8.34), can be mapped exactly onto a spin-$\frac{1}{2}$ model, and neglecting boundary terms which are unimportant for $N \to \infty$,

$$\mathcal{H} = -\frac{t}{2} \sum_{i-1}^{N} \left(\hat{\sigma}_i^x \hat{\sigma}_{i+1}^x + \hat{\sigma}_i^y \hat{\sigma}_{i+1}^y - \frac{v_1}{2t} \hat{\sigma}_i^z \hat{\sigma}_{i+1}^z - \frac{v_1}{t} \hat{\sigma}_i^z - \frac{v_1}{2t} \right). \tag{8.36}$$

Since the invention of the Bethe ansatz (Bethe, 1931), a huge number of analytical treatments of the model Eqns. (8.34) and (8.36) and its generalization have appeared so that the groundstate properties are rather well known. Here we discuss only the structure factor (a is the lattice spacing)

$$S_T(q) = \sum_{j=1}^{N} \left(\langle \hat{n}_i \hat{n}_{i+j} \rangle_T - \langle \hat{n}_i \rangle_T \langle \hat{n}_{i+j} \rangle_T \right) \cos(jqa) \tag{8.37}$$

for $T = 0$ and half filling ($\rho = 1/2$). At $v_1 = 2t$ a metal–insulator transition occurs (Ovchinnikov, 1973): for $v_1 < 2t$ there is no energy gap between the groundstate energy and the first excited states, and the system is a metal; $S(q)$ then has a peak at $q = \pi/a$ with finite width. If $v_1 > 2t$ there is a gap and the groundstate has long range order, which implies that $S(q)$ has a delta function (for $N \to \infty$) at $q = \pi/a$. For $v_1 \to \infty$ the groundstate approaches simply that of the classical model where every second lattice site is occupied and every other lattice site is empty. A related quantity of interest is the static wavevector-dependent 'susceptibility' ($\hat{\varphi}_q$ is the Fourier component of the density operator $\hat{n}_i$)

$$\chi(q) = \frac{1}{\hbar} \int_0^{\hbar/k_B T} dx \left[\left\langle e^{x\mathcal{H}} \hat{\varphi}_q e^{-x\mathcal{H}} \hat{\varphi}_{-q} \right\rangle_T - \left\langle \hat{\varphi}_{q=0} \right\rangle_T^2 \right]. \tag{8.38}$$

If $[\mathcal{H}, \hat{\rho}_q] = 0$, we would simply recover the classical fluctuation relation $\chi(q) = S_T(q)/k_B T$ since $S_T(q) = \langle \hat{\rho}_q \hat{\rho}_{-q} \rangle_T - \langle \hat{\rho}_{q=0} \rangle_T^2$. Thus, in calculating response functions $\chi(q)$ describes the response of the density to a wavevector-dependent 'field' coupling linearly to the density) one must carefully consider the appropriate quantum mechanical generalizations of fluctuation formulae, such as Eqn. (8.38).

In order to bring the problem, Eqn. (8.34) or Eqn. (8.36), into a form where the application of the Trotter formula, Eqn. (8.20), is useful, we have to find a suitable decomposition of $\mathcal{H}$ into $\mathcal{H}_1$ and $\mathcal{H}_2$. When we wish to describe the states in the occupation number representation (or the corresponding spin representation: $|S_1 \ldots S_i \ldots S_N\rangle$ means that $S_i = 1(-1)$ if the site i is occupied (empty)), we have the problem that the non-diagonal first term in Eqn. (8.34) couples different sites. Thus, one uses a decomposition where one introduces two sublattices, $\mathcal{H}_{i,j} = -t(\hat{c}_i^+ \hat{c}_j + \hat{c}_j^+ \hat{c}_i) + v_1 \hat{n}_i \hat{n}_j$, following Barma and Shastry (1977)

$$\mathcal{H}_1 = \sum_{i=1}^{N/2} \mathcal{H}_{2i-1,2i}, \qquad \mathcal{H}_2 = \sum_{i=1}^{N/2} \mathcal{H}_{2i,\,2i+1}. \tag{8.39}$$

Of course, here we require N to be even (only then does the system admit an antiferromagnetic groundstate with no domain wall in the limit $v_1 \to \infty$). The idea of this partitioning of the Hamiltonian is that now the terms in $\mathcal{H}_1$ all commute with each other as do the terms in $\mathcal{H}_2$, due to the local character of the Hamiltonian,

$$[\mathcal{H}_{2i-1,2i}, \mathcal{H}_{2j-1,2j}] = [\mathcal{H}_{2i,2i+1}, \mathcal{H}_{2j,2j+1}] = 0, \qquad \text{all } i, j. \tag{8.40}$$

Therefore the corresponding Trotter approximation reads

$$\begin{aligned} Z_P = \mathrm{Tr}[&\exp(-\mathcal{H}_{1,2}/k_B TP) \exp(-\mathcal{H}_{3,4}/k_B TP) \ldots \exp(-\mathcal{H}_{N-1,N}/k_B TP) \\ &\times \exp(-\mathcal{H}_{2,3}/k_B TP) \ldots \exp(-\mathcal{H}_{N-2,N-1}/k_B TP) \exp(-\mathcal{H}_{N,1}/k_B TP)]^P \end{aligned} \tag{8.41}$$

since Eqn. (8.40) implies that $\exp(-x\hat{\mathrm{H}}_1) = \prod_{i=1}^{N/2} \exp(-x\mathcal{H}_{i,i+1})$ and similarly for $\mathcal{H}_2$, for arbitrary x. Introducing the representation mentioned above, we need to evaluate the matrix elements

$$T(S_i, S_j; \tilde{S}_i, \tilde{S}_j) \equiv \langle S_i, S_j | \exp(-\mathcal{H}_{i,j}/k_{\mathrm{B}}TP) | \tilde{S}_i, \tilde{S}_j \rangle, \tag{8.42}$$

which yields

$$T\left(S_i, S_j; \tilde{S}_i, \tilde{S}_j\right) = \begin{pmatrix} 1 & 0 & 0 & 0 \\ 0 & \cosh(t/Pk_{\mathrm{B}}T) & \sinh(t/Pk_{\mathrm{B}}T) & 0 \\ 0 & \sinh(t/Pk_{\mathrm{B}}T) & \cosh(t/Pk_{\mathrm{B}}T) & 0 \\ 0 & 0 & 0 & \exp(-v_1/Pk_{\mathrm{B}}T) \end{pmatrix} \tag{8.43}$$

where the lines of the matrix are ordered according to the states $|-1, -1\rangle$, $|1, -1\rangle$, $|-1, 1\rangle$, and $|1, 1\rangle$, from above to below, respectively. Then the Trotter approximation for the partition function becomes (de Raedt and Lagendijk, 1985)

$$\begin{aligned} Z_P = \sum_{\{S_i^{(S)}\}}{}' \sum_{\{\tilde{S}_i^{(S)}\}}{}' \prod_{s=1}^{P} & T\left(S_1^{(s)}, S_2^{(s)}; \tilde{S}_1^{(s)}, \tilde{S}_2^{(s)}\right) \cdots \\ & \times T\left(S_{N-1}^{(s)}, S_N^{(s)}; \tilde{S}_{N-1}^{(s)}, \tilde{S}_N^{(s)}\right) \times T\left(\tilde{S}_2^{(s)}, \tilde{S}_3^{(s)}; \tilde{S}_2^{(s+1)}, \tilde{S}_3^{(s+1)}\right) \cdots \\ & \times T\left(\tilde{S}_{N-2}^{(s)}, \tilde{S}_{N-1}^{(s)}; \tilde{S}_{N-2}^{(s+1)}, \tilde{S}_{N-1}^{(s+1)}\right) \\ & \times T\left(\tilde{S}_N^{(s)}, \tilde{S}_1^{(s)}; \tilde{S}_N^{(s+1)}, \tilde{S}_1^{(s+1)}\right)\left(1 - \left|S_1^{(s)} - S_N^{(s)}\right|\right)^{N+1}. \end{aligned} \tag{8.44}$$

The primes on the summation signs in Eqn. (8.44) mean that the sums over the variables S and $\tilde{S}$ are restricted, because the total number N of fermions is fixed, i.e. $\sum_{i=1}^{N} S_i^{(s)} = \sum_{i=1}^{N} \tilde{S}_i^{(s)} = 2\mathcal{N} - N$ for all s. The last line in Eqn. (8.44) represents the physical situation in which a particle moves from site 1 to site N and vice versa. Such moves destroy the ordering in which the fermions have been created from the vacuum state. Therefore the last factor is a correction term which results from reordering the fermion operators, taking into account the anticommutation rules. Obviously, there are only negative contributions to Z_P if $\mathcal{N}$ is even, and no minus signs would be present if there were free boundary conditions, because then the entire last line of Eqn. (8.44) would be missing.

8.3.4 An intermezzo: the minus sign problem

For an interpretation of Z_P as the trace of an equivalent classical Hamiltonian, $Z_P = \mathrm{Tr}\exp(-\mathcal{H}_{\mathrm{eff}}^{(P)}/k_{\mathrm{B}}T)$, it is clearly necessary that all terms that contribute to this partition sum are non-negative, because for a real $H_{\mathrm{eff}}^{(P)}$ the term $\exp(-\mathcal{H}_{\mathrm{eff}}^{(P)}/k_{\mathrm{B}}T)$ is never negative. The anticommutation rule of fermion operators leads to negative terms, as they occur in Eqn. (8.44) for even N, and

this problem hampers quantum Monte Carlo calculations, in a very severe way. Of course, the same problem would occur if we simply tried to work with the Fermi equivalent of Z_B in Eqn. (8.15), since then the eigenfunctions $\phi_\alpha(\mathbf{R})$ are antisymmetric under the permutation of particles,

$$\hat{A}\phi_\alpha(\mathbf{R}) = \frac{1}{N!}\sum_P (-1)^P \phi(\hat{P}\mathbf{R}), \tag{8.45}$$

where $(-1)^P$ is negative if the permutation is odd, while Eqn. (8.14) did not lead to any such sign problems.

Now it is possible to generalize the Metropolis importance sampling method to cases where a quantity $\rho(x)$ in an average (x stands here symbolically for a high-dimensional phase space)

$$\langle \hat{A} \rangle = \int A(x)\,\rho(x)dx \Big/ \int \rho(x)\,dx \tag{8.46}$$

is not positive semi-definite, and hence does not qualify for an interpretation as a probability density. The standard trick (de Raedt and Lagendijk, 1981) amounts to working with $\tilde{\rho}(x) = |\rho(x)|/\int |\rho(x)|dx$ as probability density for which one can do importance sampling, and to absorb the sign of $\rho(x)$ in the quantity that is sampled. Thus

$$\langle \hat{A} \rangle = \frac{\int A(x)\mathrm{sign}(\rho(x))\tilde{\rho}(x)dx}{\int \mathrm{sign}(\rho(x))\tilde{\rho}(x)dx} = \frac{\langle \hat{A}\hat{s} \rangle}{\langle \hat{s} \rangle}, \tag{8.47}$$

where $\hat{s}$ is the sign operator that corresponds to the function sign $(\rho(x))$. While Eqn. (8.47) seems like a general solution to this so-called 'minus sign problem', in practice it is useful only for very small particle number N. The problem is that *all* regions of phase space are important but have contributions which tend to cancel each other. In practice this leads to the problem that $\langle \hat{s} \rangle$ is extremely small, huge cancellations occur in both $\langle \hat{A}\hat{s} \rangle$ and $\langle \hat{s} \rangle$, the statistical fluctuations then will render an accurate estimation of $\langle \hat{A} \rangle$ almost impossible. The reader may obtain some insight into this situation by examining a much simpler problem which presents the same difficulty, namely the evaluation of the integral

$$F(\alpha, x) = \int_{-\infty}^{\infty} e^{-x^2} \cos(\alpha x)\,dx \tag{8.48}$$

in the limit that $\alpha \to \infty$. The argument of this integral oscillates rapidly for large α and the determination of the value by Monte Carlo methods, see Chapter 3, becomes problematical. In the example given below we show how the determination of the value of the integral becomes increasingly imprecise as α increases. For $\alpha = 0$ the estimate after 10^7 samples is good to better than 0.03%, whereas for $\alpha = 4$ the fluctuations with increasing sampling are of the

order of 1%. For larger values of α the quality of the result deteriorates still more.

Example

Use simple sampling Monte Carlo to estimate $F(\alpha, x)$ for $x = 0, 1.0, 2.0, 4.0$:

	α			
Number of points	0	1.0	2.0	4.0
10 000 000	0.885 717 0	0.688 967 0	0.325 109 0	0.016 047 0
20 000 000	0.886 325 5	0.689 699 0	0.325 827 5	0.016 436 0
30 000 000	0.886 106 0	0.689 621 0	0.325 403 7	0.015 922 3
40 000 000	0.885 929 5	0.689 765 3	0.325 628 3	0.016 033 8
50 000 000	0.886 271 8	0.690 020 8	0.325 923 2	0.016 206 6
60 000 000	0.886 562 6	0.690 204 5	0.325 984 2	0.016 246 7
70 000 000	0.886 407 4	0.690 090 4	0.325 772 1	0.016 037 0
80 000 000	0.886 347 0	0.690 090 5	0.325 786 0	0.015 939 5
90 000 000	0.886 206 9	0.689 879 8	0.325 688 7	0.015 898 8
100 000 000	0.886 201 2	0.689 889 0	0.325 741 1	0.016 048 8
Exact	0.886 226 6	0.690 194 0	0.326 024 5	0.016 231 8

Another very important quantum problem in which progress has been limited because of the minus sign problem is the Hubbard Hamiltonian (Hubbard, 1963),

$$\mathcal{H}_{\text{Hubbard}} = t \sum_{\langle i,j \rangle} \left(\hat{c}^{+}_{i,\sigma} \hat{c}_{j,\sigma} + \hat{c}^{+}_{j,\sigma} \hat{c}_{i,\sigma} \right) + U \sum_{i} \hat{n}_{i\downarrow} \hat{n}_{i\uparrow} \tag{8.49}$$

where $\hat{c}^{+}_{i,\sigma}(\hat{c}_{i,\sigma})$ creates (annihilates) a fermion of spin $\sigma = \uparrow,\downarrow$ at site i, t is the hopping matrix element analogously to Eqn. (8.34), while U represents the on-site Coulomb interaction strength. The minus sign problem has been studied in detail, and it was found that (Loh *et al.*, 1990)

$$\langle \hat{s} \rangle \propto \exp(-\gamma NU/k_{\text{B}}T), \tag{8.50}$$

where γ is a constant that depends strongly on the filling of the band. It is obvious that the minus sign problem gets worse as N increases and as the temperature is lowered. Finding methods to avoid this problem (or at least to make γ very small) is still an active area of research.

8.3.5 Spinless fermions revisited

While the minus sign problem is also a severe problem for the Hamiltonian Eqn. (8.34) in $d = 2$ and 3 dimensions, for $d = 1$ the only remnant of this problem is the last factor on the right-hand side of Eqn. (8.44), and this is clearly not a big problem (note that this term would be completely absent for the choice of free boundary conditions).

The first step in dealing with Eqn. (8.44) is the elimination of the $\tilde{S}_i^{(s)}$ variables, which can be done analytically. Note that $T(S_i,\ S_j;\ \tilde{S}_i,\ \tilde{S}_j)$ from Eqn. (8.43) can be rewritten as

$$T(S_i, S_j; \tilde{S}_i, \tilde{S}_j) = \delta_{S_i S_j, \tilde{S}_i \tilde{S}_j} T_{S_i, S_j}(S_i, S_i; \tilde{S}_i, \tilde{S}_j), \tag{8.51}$$

where the remaining (2×2) matrices $T_1(S,\ \bar{S})$ and $T_{-1}(S, \bar{S})$ are

$$T_1(S,\ \bar{S}) \equiv \begin{pmatrix} 1 & \cosh(t/k_B TP) \\ \cosh(t/k_B TP) & \exp(-\upsilon_1/k_B TP) \end{pmatrix}, \tag{8.52}$$

where the upper line refers to state $|-1\rangle$ and the lower line to state $|1\rangle$, and

$$T_{-1}(S, \bar{S}) \equiv \delta_{S,\bar{S}} \sinh(t/k_B TP). \tag{8.53}$$

Summing over the $\tilde{S}_i^{(s)}$ in Eqn. (8.44) then yields

$$Z_P = \sum_{\{S_i^{(s)}\}} \sum_{\{\sigma_j\}} \prod_{j=1}^{P} T_{\sigma_j \phi_1^{(j)}}\left(S_1^{(j)}, \sigma_j \phi_1^{(j)} S_2^{(j)}\right) T_{\sigma_j \phi_2^{(j)}}\left(\sigma_j \phi_2^{(j)} S_2^{(j)}, S_3^{(j+1)}\right) \cdots$$
$$T_{\sigma_j \phi_{N-1}^{(j)}}\left(S_{N-1}^{(j)}, \sigma_j \phi_{N-1}^{(j)} S_N^{(j)}\right) T_{\sigma_j \phi_N^{(j)}}\left(\sigma_j \phi_{N,j}^{(j)} S_N^{(j)}, S_1^{(j+1)}\right) \sigma_j^{N+1} \delta_{\phi_N^{(j)},1}, \tag{8.54}$$

where $\{\phi_\ell^{(j)}\}$ are the string-like variables formed from the $\{S_i^{(s)}\}$,

$$\phi_\ell^{(j)} = \prod_{i=1}^{\ell} S_i^{(j)} S_i^{(j+1)}. \tag{8.55}$$

Therefore, the effective lattice model, $H_{\text{eff}}^{(P)}$ that results from Eqn. (8.54), $Z_P \equiv \text{Tr}\ \exp(-\mathcal{H}_{\text{eff}}^{(P)}/k_B T)$, contains non-local interactions both along the chain and in the Trotter imaginary time direction, unlike the Ising model in a transverse field, that had non-local interactions in the Trotter direction only. The total number of variables in Eqn. (8.54) is $P(N+1)$, namely the PN spins $\{S_i^{(s)}\}$ and P variables $\sigma_j = \pm 1$. The extra sum over the latter is a consequence of the use of periodic boundary conditions. If we work with free boundary conditions, this sum can be omitted in Eqn. (8.54) and we can put $\sigma_j \equiv 1$ there and no negative terms occur. Even then a Monte Carlo process that produces states proportional to the Boltzmann weight $\exp(-\mathcal{H}_{\text{eff}}^{(P)}/k_B T)$ is difficult to construct. To avoid the non-local interaction in the spatial direction generated in Eqn. (8.54), one can rather attempt to construct a Monte Carlo scheme that realizes the Boltzmann weight for Eqn. (8.44), at the expense that one has twice as many variables ($S_i^{(s)}$ and $\tilde{S}_i^{(s)}$, respectively). However, the zero matrix elements in Eqn. (8.43) imply that many states generated would have exactly zero weight if one chose trial configurations of the $\{S_i^{(s)},\ \tilde{S}_i^{(s)}\}$ at random: rather the Monte Carlo moves have to be constructed such that the Kronecker delta in Eqn. (8.51) is never zero. This constraint can be realized by two-particle moves in the checkerboard representation, Fig. 8.11, as proposed by Hirsch *et al.* (1982). Figure 8.12 shows the type of results that can be obtained from this

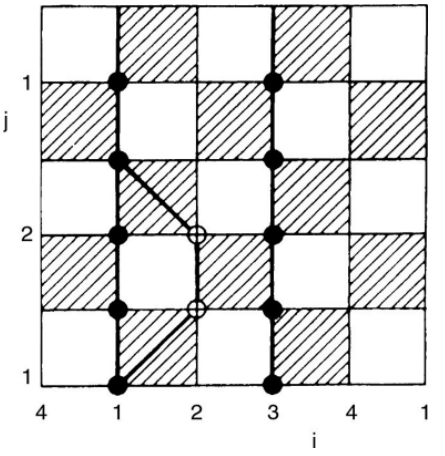

Fig. 8.11 Example of the elementary two-particle jump procedure for the checkerboard lattice, for a chain of four sites. Each shaded square represents a T-matrix and determines which particles can interact with each other (only particles that sit on the corners of the same shaded square). The variables $S_i^{(j)}$ are defined on the rows $j = 1, 2$ whereas the variables $\tilde{S}_i^{(j)}$ are defined on the rows between the $j = 1$ and $j = 2$ rows (note we have chosen $P = 2$ here, and we *must* impose periodic boundary conditions in the Trotter direction because of the trace operation; the figure implies also the choice of periodic boundary conditions in the spatial direction as well). The black dots indicate a state of the lattice with non-zero weight, representing particles present in the occupation number representation (the thick lines connecting them are the so-called 'world lines'). A trial state is generated by moving two particles from one vertical edge of an *unshaded* square to the other. From de Raedt and Lagendijk (1985).

method. One can see from Fig. 8.12 that non-trivial results for this fermion model in $d = 1$ dimensions have been obtained, but even in this case it is difficult to go to large N (the largest size included in Fig. 8.12 is $N = 100$), and statistical errors are considerable at low temperatures. Nevertheless Fig. 8.12 gives reasonable evidence for the quite non-trivial scaling dependence $S(\pi) \propto \ln N$.

This case of fermions in $d = 1$ has again shown that the PIMC methods always need some thought about how best to split the Hamiltonian into parts so that, with the help of the Trotter formalism, one can derive a tractable $\mathcal{H}_{\text{eff}}$. Finding efficient Monte Carlo moves also is a non-trivial problem. Of course, since the steps described in the present section the subject has been pushed much further. We direct the interested reader to the reviews quoted in the introduction for more recent work and details about specialized directions.

8.3.6 Cluster methods for quantum lattice models

In Chapter 5 we saw that for many kinds of classical models there were some specialized techniques that could be used to effectively reduce the correlation times between configurations which have been generated. The constraints on direct application of these methods to the classical models which result from the Trotter–Suzuki transformation arise due to the special constraints on which

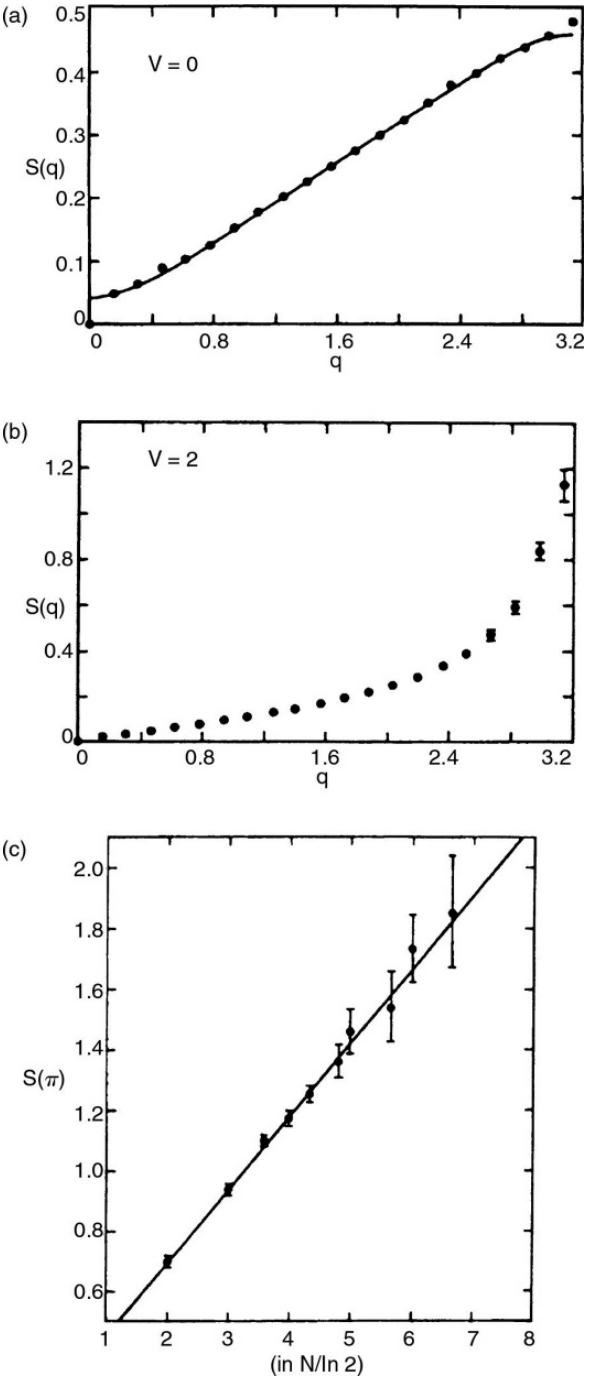

Fig. 8.12 (a) Points showing Monte Carlo data for the structure factor for a 40-site lattice containing 20 non-interacting electrons ($t = 1$, $V = 0$) at low temperature, $1/k_B T = 4$. Solid line is the analytical solution for this system. (b) Monte Carlo results for the structure factor for $t = 1$ and $V = 2$ at $1/k_B T = 4$. Note the difference in scale between parts (a) and (b). (c) Structure factor $S(q = \pi)$ for the half-filled case with $\upsilon/2t = 1$ vs. the lattice size. From Hirsch *et al*. (1982).

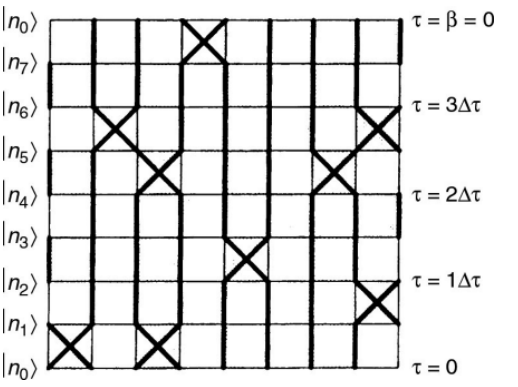

Fig. 8.13 Possible loop structure for the lattice produced using the Trotter formula for a one-dimensional $S = \frac{1}{2}$ Heisenberg model. Note that there are periodic boundary conditions applied in both the real space and Trotter directions. From Gubernatis and Kawashima (1996).

spins may be overturned. Evertz and coworkers (1993) have introduced a form of the cluster algorithm, known as the 'loop algorithm', which addresses these difficulties. It is basically a world-line formulation that employs non-local changes. We have already mentioned that the transformed spin models are equivalent to vertex models in which every bond contains an arrow which points parallel or anti-parallel to a direction along the bond. Thus, in two dimensions each vertex is the intersection of four arrows which obey the constraints that there must be an even number of arrows flowing into or out of a vertex and that they cannot all point either towards or away from the vertex. A 'loop' is then an oriented, closed, non-branching path of bonds, all of which contain arrows which point in the same direction. This path may be self-intersecting. A 'flip' then reverses all arrows along the loop. How are the loops chosen? One begins with a randomly chosen bond and looks to the vertex to which it points. There will be two outgoing arrows and one then needs to decide which arrow the loop will follow; this depends upon the model in question. An example of a possible loop configuration is shown in Fig. 8.13. For some models it is also possible to define improved estimators in terms of the 'cluster' properties just as was done for simple classical spin models.

The method was further generalized to arbitrary spin value by Kawashima and Gubernatis (1995) and we refer the reader there (or to Gubernatis and Kawashima (1996), Kawashima (1997)) for more details.

8.3.7 Continuous time simulations

The lowest temperature that can be reached using the path integral/Trotter–Suzuki decomposition methods is dependent upon the number of time slices that are introduced. To go to the continuum limit in time, i.e. infinite Trotter index, one needs to imagine producing increasingly fine granularity in time, i.e. the plaquettes approach infinitesimal length in the time direction. A continuous time algorithm is the limit of this process and offers the advantage that one does not need to store all spins states in the time direction but rather only the initial state (at time $t = 0$) plus the transition times for each spin site (Beard and Wiese, 1996). Thus, the continuous time algorithm eliminates one

of the most severe sources of systematic error and removes the excess burden of performing multiple simulations with different numbers of time slices in order to attempt to extrapolate to the infinite limit. Although the original implementation was demonstrated for a Heisenberg antiferromagnet on a square lattice, the continuous-time formulation can be applied to a wide range of problems and does not rely on the use of a particular sampling algorithm, e.g. 'cluster flipping'. For a detailed description of this algorithm and some of its applications, we recommend that the reader consult the review by Gull *et al.* (2011).

8.3.8 Decoupled cell method

A different approach was proposed by Homma *et al.* (1984, 1986). The system is divided into a set of 'cells' consisting of a center spin i and a symmetric set of surrounding neighbors. The energies of the different states of the cell are solved for as an eigenvalue problem of the cell portion of the Hamiltonian and then Monte Carlo sampling is carried out, i.e. spin-flipping, using relative probabilities of these cell states. The size of the cell is then systematically increased to allow extrapolation to the full lattice.

To examine this method more formally we begin by expressing s_i as the state of the central spin i in a cell, S_i as the state of all other spins in the cell, and $\overline{S}_i$ as the state of all spins outside the cell. The transition probability between state $S = (s_i, S_i, \overline{S}_i)$ and $S' = (-s_i, S_i, \overline{S}_i)$ is

$$q(S) = \frac{P(S)}{P(S')} = \frac{\langle S|\exp(-\beta\mathcal{H})|S\rangle}{\langle S'|\exp(-\beta\mathcal{H})|S'\rangle} \tag{8.56}$$

and this is then approximated by

$$q^{(v)}(S) = \frac{\langle s_i S_i|\exp(-\beta\mathcal{H}(v,\ i)|s_i S_i\rangle}{\langle -s_i S_i|\exp(-\beta\mathcal{H}(v,\ i)|-s_i S_i\rangle} \tag{8.57}$$

where $\mathcal{H}(v, i)$ is the cell Hamiltonian for a cell of size v. The transition probability is then simply

$$W_{\mathrm{DC}}(-s_i \rightarrow s_i) = \max[1, q^{(v)}(S_i)]. \tag{8.58}$$

This procedure has been used successfully for a number of different quantum spin systems, but at very low temperatures detailed balance begins to break down and the specific heat becomes negative. A modified version of the decoupled cell method was introduced by Miyazawa *et al.* (1993) to remedy this problem. The improvement consists of dividing the system into overlapping cells such that every spin is at the center of some cell and then using all cells which contain spin i, to calculate the flipping probability instead of just one cell in which the ith spin was the center. Miyazawa and Homma (1995) provide a nice overview of the enhanced method and describe a study of the $\mathcal{J}_1 - \mathcal{J}_2$ model using this approach The decoupled cell method was also used to study the quantum XY-model on a triangular lattice using systems as large as 45×45

and seven-spin cells. Typically 10^4 Monte Carlo steps were used for equilibration and between 10^4 and 8×10^4 were used for averaging. Both groundstate properties and temperature-dependent thermal properties were studied.

8.3.9 Handscomb's method and the stochastic series expansion (SSE) approach

An alternative method with a completely different philosophy was suggested by Handscomb (1962, 1964). Although it has been used for a rather limited range of problems, we mention it here for completeness. For simplicity, we describe this approach in terms of a simple linear $S = \frac{1}{2}$ Heisenberg chain of N spins whose Hamiltonian we re-express in terms of permutation operators $E(i, j) = (1 + \hat{S}_i \cdot \hat{S}_j)/2$

$$\mathcal{H} = -\mathcal{J} \sum_{i=1}^{N} E\,(i, i+1) + \tfrac{1}{2}\mathcal{J}N. \tag{8.59}$$

The exponential in the partition function is then expanded in a power series in $\beta\mathcal{H}$ to yield

$$\begin{aligned} Z &= \sum_{n=0}^{\infty} \mathrm{Tr}\{(\beta\mathcal{H})^n\} \\ &= \sum_{n=0}^{\infty} \sum_{C_n} \frac{1}{n!} \mathrm{Tr}\{\mathcal{H}_{i_1} \cdots \mathcal{H}_{i_n}\} \\ &= \sum_{n=0}^{\infty} \sum_{C_n} \frac{K^n}{n!} \mathrm{Tr}\{P(C_n)\} \end{aligned} \tag{8.60}$$

where $K = \beta\mathcal{J}$ and the second sum is over all possible products $P(C_n)$ with n operators $E(i, i+1)$. The distribution function can then be expressed as

$$\pi(C_n) = \frac{K^n}{n!} \mathrm{Tr}\{P(C_n)\}. \tag{8.61}$$

The Monte Carlo process then begins with an arbitrary sequence of permutation operators. A trial step then consists of either adding an operator to a randomly chosen place in the sequence or deleting a randomly chosen operator from the sequence subject to the condition of detailed balance,

$$P(C_{n+1} \to C_n)\pi(C_{n+1}) = P(C_n \to C_{n+1})\pi(C_n), \tag{8.62}$$

where P_i is the probability of choosing an operator. This approach has been successfully applied to several quantum Heisenberg models by Lyklema (1982), Lee *et al.* (1984), Gomez-Santos *et al.* (1989), and Manousakis and Salvador (1989). Studies of Heisenberg chains used 2×10^5 Monte Carlo steps for equilibration and as many as 5×10^6 Monte Carlo steps for statistical averaging. Lee *et al.* (1984) have modified the approach by shifting the zero of the energy with the result that only terms with an even number of operators give non-zero

trace, a modification which helps to largely overcome the minus sign problem in antiferromagnetic quantum Heisenberg models studied by this method. Note that this approach does not make the problem trivial; the study of 32×32 square lattice systems still required 6×10^6 Monte Carlo steps. Sandvik and Kurkijärvi (1991) later introduced a further generalization which is applicable to any spin length.

The crucial difference between the method by Sandvik and Kurkijärvi (1991) and the original Handscomb method, sketched above, is that in the high temperature series expansion, Eqn. (8.60), the sampling is done in a combined space of spin states and index sequences. Thus, there is no longer the need to compute the traces of the products of the Hamiltonian written in Eqn. (8.60) explicitly. Unlike methods based on the Trotter decomposition in imaginary time where the discreteness of the time step of $\delta\tau$ causes a systematic error, this method in principle is free of systematic errors, and has now become rather popular. It is commonly referred to as the 'stochastic series expansion' (SSE) algorithm (Sandvik, 1992, 1997) and is essentially a Quantum Monte Carlo method working in continuous rather than discrete imaginary time. The actual implementation is somewhat technical, however, and hence will not be described here. An important advantage of this approach is also that it can be combined with either 'simulated tempering' (Marinari and Parisi 1992) or 'parallel tempering' (see Section 5.4.2), and in this way a much more economical use of computer resources for simulations of quantum spin systems has become possible. As an example of an application, we mention the finite size scaling study (similar to the one described in Section 4.2.3) of the critical behavior of the phase transition of the three-dimensional $S = ½$ Quantum Heisenberg antiferromagnet (Sandvik, 1998). It was found that the critical temperature occurs at $k_B T_c/\mathcal{J} = 0.946 \pm 0.001$, and the critical exponents are compatible with their values in the classical limit ($S \to \infty$), as expected. However, the largest accessible lattice size was only $L = 16$, and thus 'high resolution' studies of phase transitions (as are possible for classical systems, see Section 7.2) are still challenging for quantum systems.

8.3.10 Wang–Landau sampling for quantum models

Although the Wang–Landau sampling algorithm described in Chapter 5 would at first glance seem to be inapplicable for quantum systems, Troyer *et al.* (2003) showed how a clever modification of perspective could enable use of the method. They start by expressing the partition function as a high temperature expansion

$$Z = \sum_{n=0}^{\infty} \frac{\beta^n}{n!} \mathrm{Tr}(-\mathcal{H})^n \equiv \sum_{n=0}^{\infty} g(n)\beta^n \tag{8.63}$$

where $\beta = (1/k_B T)$. The nth order series coefficient $g(n)$ will play the role of the density of states in the original (classical) version of the algorithm. The quantum algorithm then performs a random walk in the space of series

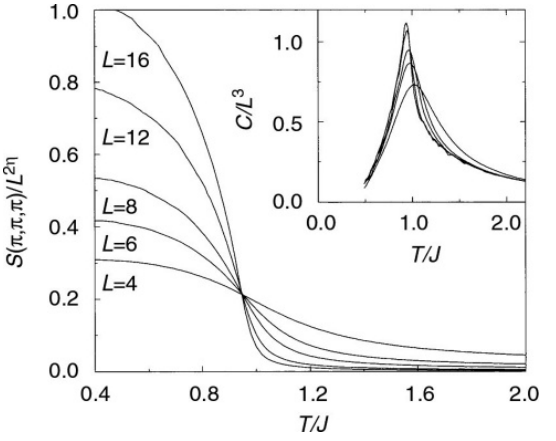

Fig. 8.14 Scaling plot of the structure factor at the Brillouin zone boundary for a cubic antiferromagnet as a function of temperature. The inset shows the specific heat. The cutoff $\Lambda = 500(L/4)^3$ limits the calculation to $k_B T \geq 0.4\mathcal{J}$. After Troyer *et al*. (2003).

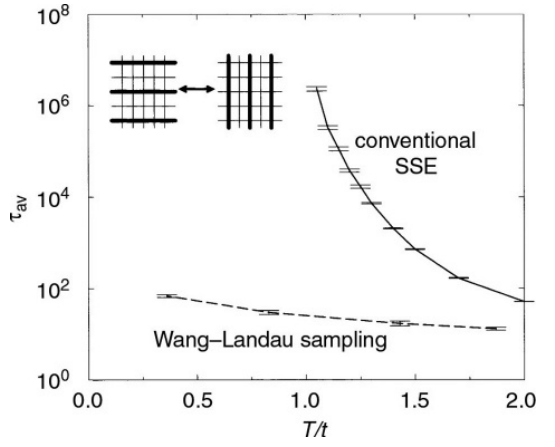

Fig. 8.15 Average tunneling times between horizontal and vertical arrangement of strips in a hard-core Boson model. Comparison is made to results from the stochastic series expansion method (SSE). After Troyer *et al*. (2003).

expansion coefficients, monitors the histogram in their orders n, and determines coefficients $g(n)$. When $g(n)$ is determined to sufficient precision it is then used, via Eqn. (8.63) to determine the thermodynamic properties. As an example, in Fig. 8.14 we show the temperature dependence of the structure factor at the Brillouin zone boundary (related to the staggered susceptibility) for a Heisenberg antiferromagnet on an $L \times L \times L$ simple cubic lattice. Quite precise data can be obtained in this manner using modest computer resources (a few days on an 800 MHz Pentium-III CPU).

This algorithm was also applied to the study of a first order transition in a two-dimensional hard-core Boson model. At low temperature and half filling the ordered state consists of stripes that can run either horizontally or vertically. The tunneling times between these two equivalent configurations can be greatly reduced using the quantum version of Wang–Landau sampling, as shown in Fig. 8.15.

A very different approach can be followed to allow study of quantum phase transitions, i.e. at $T = 0$. Instead of scanning a temperature range one can

vary the interactions at constant temperature. If we define the Hamiltonian by $\mathcal{H} = \mathcal{H}_o + \lambda V$, we can rewrite the partition function

$$Z = \sum_{n=0}^{\infty} \frac{\beta^n}{n!} \mathrm{Tr}(-\mathcal{H}_o - \lambda V)^n = \sum_{n_\lambda=0}^{\infty} \tilde{g}(n_\lambda)\lambda^{n_\lambda} \tag{8.64}$$

and a very similar sampling approach can be used as for Eqn. (8.63).

From the two examples discussed above, we see again, then, that an intelligent use of algorithms is often far more powerful than brute force.

8.3.11 Fermion determinants

Since it is so hard to deal with fermionic degrees of freedom in quantum Monte Carlo calculations directly, it is tempting to seek methods where one integrates over fermionic degrees of freedom analytically, at the expense of having to simulate a problem with a much more complicated Hamiltonian (Blanckenbecler *et al.*, 1981). This route is, for instance, followed in simulations dealing with lattice gauge theory, see Chapter 11, where one has to deal with a partition function

$$Z = \int \mathcal{D}A_\mu \mathcal{D}\overline{\Psi}\mathcal{D}\Psi \exp[S(A_\mu, \overline{\Psi}, \Psi)] \tag{8.65}$$

where A_μ denotes the gauge fields (μ denotes Cartesian coordinates in the four-dimensional Minkowski space), and $\overline{\Psi}$, Ψ stand for the particle fields (indices $f = 1, \ldots, n_f$ for the 'flavors' and $c = 1, \ldots, n_c$ for the 'colors' of these quarks are suppressed). Now quantum chromodynamics (QCD) implies that the action S is bilinear in $\overline{\Psi}$, Ψ and hence can be written as ($\hat{M}$ is an operator that need not be specified here)

$$S(A_\mu, \overline{\Psi}, \Psi) = \frac{1}{k_B T}\mathcal{H}_0(A_\mu) - \sum_{i=1}^{n_f} \overline{\Psi}\hat{M}\Psi. \tag{8.66}$$

Here we have written the part of the action that depends on gauge fields only as $(1/k_B T)\mathcal{H}_0$, to make the analogy of QCD with statistical mechanics explicit. Note that this formulation is already approximate, since one uses one-component fields (so-called 'staggered fermions' rather than four-component Dirac spinors) here. Now it is well known that the path integration over the fermionic fields (remember these are anticommuting variables) can be integrated out to yield

$$\begin{aligned} Z &= \int \mathcal{D}A_\mu (\det \hat{M})^{n_f} \exp[-\mathcal{H}_0(A_\mu)/k_B T] \\ &= \int \mathcal{D}A_\mu \exp[-\mathcal{H}_{\mathrm{eff}}(A_\mu)/k_B T] \\ \mathcal{H}_{\mathrm{eff}}(A_\mu) &= \mathcal{H}_0(A_\mu) - \frac{n_f}{2}\ln[\det(\hat{M}^+\hat{M})]. \end{aligned} \tag{8.67}$$

In the last step (det $\hat{M}$) was replaced by $[\det(\hat{M}^{+}\hat{M})]^{1/2}$, provided the determinant is positive-definite. Unfortunately, this condition is satisfied only in special cases with 'particle-hole' symmetry, e.g. QCD in a vacuum or the simplest Hubbard model at half filling. While $\mathcal{H}_0(A_\mu)$ in the lattice formulation of QCD is local, see Chapter 11, the above determinant introduces a non-local interaction among the A_μ.

In condensed matter problems such as the Hubbard Hamiltonian this method does not work directly, since in addition to the bilinear term in the fermion operators $t\hat{c}^{+}_{i\sigma}\hat{c}_{j\sigma}$ (describing hopping of an electron with spin $\sigma = \uparrow, \downarrow$ from site i to site j) one also has the on-site interaction $U\hat{n}_{i\uparrow}\hat{n}_{i\downarrow} = U\hat{c}^{+}_{i\uparrow}\hat{c}_{i\uparrow}\hat{c}^{+}_{i\downarrow}\hat{c}_{i\downarrow}$. However, it is still possible to eliminate the fermionic degrees of freedom from the partition function by introducing auxiliary (bosonic) fields. The key element of this step is the relation

$$\int_{-\infty}^{+\infty} e^{-a\phi^2 - b\phi}\, d\phi = \sqrt{\frac{\pi}{a}}\, e^{-b^2/4a}, \qquad a > 0. \tag{8.68}$$

Thus a variable b appearing quadratic in the argument of an exponential can be reduced to a linear term (the term $b\phi$ on the left-hand side of the above equation) but on the expense of an integration over the auxiliary variable ϕ. This trick then yields for the on-site interaction of the Hubbard model for $U > 0$

$$\exp\left(-\frac{U}{k_{\mathrm{B}}TP}\sum_{\ell=1}^{N}\hat{n}_{\ell\uparrow}\hat{n}_{\ell\downarrow}\right) \propto \prod_{\ell=1}^{N}\int_{-\infty}^{+\infty} d\phi_\ell \exp\left[-\frac{Pk_{\mathrm{B}}T\phi_\ell^2}{2U} - \phi_\ell(\hat{n}_{\ell\uparrow} - \hat{n}_{\ell\downarrow}) - \frac{U(\hat{n}_{\ell\uparrow} + \hat{n}_{\ell\downarrow})}{2k_{\mathrm{B}}TP}\right]. \tag{8.69}$$

Using this expression in the framework of the Trotter decomposition, one then can carry out the trace over the fermionic degrees of freedom and again obtain a determinant contribution to the effective Hamiltonian that is formulated in terms of the $\{\phi_\ell\}$, the auxiliary boson fields.

Of course, these remarks are only intended to give readers the flavor of the approach, and direct them to the original literature or more thorough reviews (e.g. de Raedt and von der Linden, 1992) for details.

8.4 MONTE CARLO METHODS FOR THE STUDY OF GROUNDSTATE PROPERTIES

For some quantum mechanical many-body problems even understanding the groundstate is a challenge. A famous example (which is of interest for the understanding of high-T_c superconductivity in the CuO_2 planes of these perovskitic materials) is the groundstate of the spin $-\frac{1}{2}$ Heisenberg antiferromagnet on

the square lattice. While for the Ising model the problem is trivial – with a nearest neighbor interaction the lattice simply is split in two ferromagnetic sublattices in a checkerboard fashion, on one sublattice spins are up, on the other they are down. This so-called Néel state is not a groundstate of the Heisenberg antiferromagnet.

Various methods have been devised to deal with problems of this kind, e.g. diffusion Monte Carlo (DMC) methods (see Badinski and Needs, 2007), variational Monte Carlo (VMC) methods, Green's function Monte Carlo (GFMC), and projector quantum Monte Carlo (PQMC). In the following, we only sketch some of the basic ideas, following de Raedt and von der Linden (1992).

8.4.1 Variational Monte Carlo (VMC)

The starting point of any VMC calculation is a suitable trial wave function, $|\Psi^T\{m\}\rangle$, which depends on a set of variational parameters $\{m\}$. Using the fact that the problem of Heisenberg antiferromagnets can be related to the hard-core Boson problem, we describe the approach for the latter case. We write (de Raedt and von der Linden, 1992)

$$|\Psi\rangle_{\text{trial}} = \sum_{\Gamma} \exp\left\{ -\sum_{ij} \eta_{ij} \Gamma_i \Gamma_j \right\} |\Gamma\rangle \,, \tag{8.70}$$

where the summation extends over all real space configurations Γ, with $\Gamma_i = 1$ if site i is occupied and $\Gamma_i = 0$ otherwise. The expectation value for an arbitrary operator $\hat{O}$ is then

$$\langle \hat{O} \rangle = \frac{{}_{\text{trial}}\langle \Psi | \hat{O} | \Psi \rangle_{\text{trial}}}{{}_{\text{trial}}\langle \Psi | \Psi \rangle_{\text{trial}}} = \sum_{\Gamma} P(\Gamma)\, O(\Gamma) = \frac{1}{M} \sum_{\ell=1}^{M} O(\Gamma^{(\ell)}), \tag{8.71}$$

with

$$O(\Gamma) = \sum_{\Gamma} \langle \Gamma | \hat{O} | \Gamma' \rangle \exp\left\{ -\sum_{ij} \eta_{ij} (\Gamma'_i \Gamma'_j - \Gamma_i \Gamma_j) \right\}. \tag{8.72}$$

The Markov chain of real space configurations is denoted in Eqn. (8.71) as $\Gamma^{(1)}, \Gamma^{(2)}, \ldots, \Gamma^{(M)}$, M being the total number of configurations over which is sampled. Thus one can use an importance sampling method here, not with a thermal probability density $Z^{-1} \exp(-\mathcal{H}^{\text{eff}}/k_{\text{B}}T)$ but with a probability density $P(\Gamma)$ given as

$$P(\Gamma) = (Z')^{-1} \exp\left(-2 \sum_{ij} \eta_{ij} \Gamma_i \Gamma_j \right), \quad Z' = \sum_{\Gamma} \exp\left(-2 \sum_{ij} \eta_{ij} \Gamma'_i \Gamma'_j \right). \tag{8.73}$$

The energy is calculated using Eqn. (8.71) for the Hamiltonian $\mathcal{H}$ and it is minimized upon the variational parameters $\{\eta_{ij}\}$. Of course, in order that this scheme is tractable, one needs a clever ansatz with as few such parameters

as possible. A short range interaction (SR) corresponds to a wave function proposed a long time ago by Hulthén (1938), Kasteleijn (1952), and Marshall (1955):

$$\eta_{ij}^{\mathrm{SR}} = \begin{cases} \infty, & \text{if } i = j \text{ (hard-core on-site interaction)} \\ \eta, & \text{if } i, j \text{ are nearest neighbors} \\ 0, & \text{otherwise.} \end{cases} \tag{8.74}$$

The variational principle of quantum mechanics implies $\langle \mathcal{H} \rangle \geq E_0$, the groundstate energy, as is well known. Therefore, the lower energy a trial wave function $|\Psi\rangle_{\mathrm{trial}}$ yields the closer one can presumably approximate the true groundstate. It turns out that lower energies are found when one replaces the 'zero' in the last line by a long range (LR) part (Horsch and von der Linden, 1988; Huse and Elser, 1988),

$$\eta_{ij}^{\mathrm{LR}} = \alpha |\mathbf{r}_i - \mathbf{r}_j|^{-\beta}, \tag{8.75}$$

if i, j are more distant than nearest neighbors, and α, β then are additional varational parameters. All these trial wave functions lead to long range order for the two-dimensional Heisenberg antiferromagnet which is more complicated than the simple Néel state, namely the so-called 'off-diagonal long range order' (ODLRO). Another famous trial function, the 'resonant valence bond' state (RVB) originally proposed by Liang *et al.* (1988), corresponds to the choice (Doniach *et al.* (1988); p is another variational parameter)

$$\eta_{ij} = p \ln(|\mathbf{r}_i - \mathbf{r}_j|) \tag{8.76}$$

in the case where (incomplete) long range order of Néel type is admitted. Also other types of RVB trial functions exist (Liang *et al.*, 1988) which lead only to a groundstate of 'quantum liquid' type with truly short range antiferromagnetic order.

Problem 8.2 Show that the order parameter $\hat{\mathbf{M}} = \sum_i \hat{\mathbf{S}}_i$ of a quantum Heisenberg ferromagnet ($\mathcal{H} = -J \sum_{\langle i,j \rangle} \hat{\mathbf{S}}_i \cdot \hat{\mathbf{S}}_j$, for spin quantum number $S = \frac{1}{2}$, $J > 0$) commutes with the Hamiltonian. Show that the staggered magnetization (order parameter of the Néel state) does not commute with the Hamiltonian of the corresponding antiferromagnet ($J < 0$). Interpret the physical consequences of these results.

Problem 8.3 Transform the Heisenberg antiferromagnet on the square lattice, $\mathcal{H} = J \sum_{\langle i,j \rangle} \hat{\mathbf{S}}_i \cdot \hat{\mathbf{S}}_j$, into the hard-core boson Hamiltonian, $\mathcal{H} = -J \sum_{\langle i,j \rangle} \hat{b}_i^+ \hat{b}_j + J \sum_{\langle i,j \rangle} \hat{n}_i \hat{n}_j + E_0$, by using the transformations $\hat{\mathbf{S}}_i^+ = \hat{\mathbf{S}}_i^x + i\hat{\mathbf{S}}^y = \hat{\mathbf{b}}_i^+$, $\hat{\mathbf{S}}_i^- = \hat{\mathbf{S}}_i^x - i\hat{\mathbf{S}}_i^y = \hat{\mathbf{b}}_i$, and $\hat{\mathbf{S}}_i^z = \frac{1}{2} - \hat{\mathbf{b}}_i^+ \hat{\mathbf{b}}_i$, with the hard-core constraint $\hat{\mathbf{b}}_i^{+2} = 0$ and $\hat{\mathbf{b}}_i = e_i \hat{\mathbf{b}}_i$, with $e_i = 1$ on sublattice 1, $e_i = -1$ on sublattice 2, $\hat{n}_i = \hat{b}_i^+ \hat{b}_i$. Show that $E_0 = -J(N - N_b)$, where N is the number of spins and N_b is related to the z-component of the total magnetization, $N_b = N/2 - S_0^z$ ($N_b = \sum_i \langle \hat{n}_i \rangle$ is the total number of bosons).

8.4.2 Green's function Monte Carlo methods (GFMC)

The basic idea of GFMC (originally used to study the groundstate of the interacting electron gas by Ceperley and Alder (1980); it has also been extended to study the two-dimensional Heisenberg antiferromagnet, Trivedi and Ceperley (1989)) is the repeated application of the Hamiltonian $\mathcal{H}$ to an almost arbitrary state of the system, in order to 'filter out' the groundstate component. To do this, one carries out an iterative procedure

$$\left|\Psi^{(n+1)}\right\rangle = [1 - \tau\,(\mathcal{H} - \hbar\omega)]\left|\Psi^{(n)}\right\rangle = \hat{G}\left|\Psi^{(n)}\right\rangle \tag{8.77}$$

where we have written down the nth step of the iteration, and $\hbar\omega$ is a guess for the groundstate energy. Since $\hat{G}$ can be viewed as the series expansion of the imaginary time evolution operator $\exp[-\tau(\mathcal{H} - \hbar\omega)]$ or of the propagator $[1 + \tau\,(\mathcal{H} - \hbar\omega)]^{-1}$ for small steps of imaginary time τ, the notion of a Green's function for $\hat{G}$ becomes plausible.

Now the iteration converges to the groundstate only if $\tau < 2/(E_{\max} - \hbar\omega)$, $E_{\max}$ being the highest energy eigenvalue of $\mathcal{H}$, which shows that GFMC is applicable only if the spectrum of energy eigenvalues is bounded. In addition, this condition implies that τ has to decrease as $1/N$ because $E_{\max} - E_{\rm o} \propto N$. Therefore, one needs a large number of iterations with increasing system size.

In order to realize Eqn. (8.77), one expands the many-body wave function $|\Psi\rangle$ in a suitable set of many-body basis states $|R\rangle$,

$$|\Psi\rangle = \sum_R \Psi\,(R)\,|R\rangle, \tag{8.78}$$

which must be chosen such that the coefficients $\Psi(R)$ are real and non-negative, so that they can be regarded as probability densities. In the hard-core boson problem described above (Problem 8.3), one can write explicitly

$$|R\rangle = \prod_{\ell=1}^{N_b} \hat{\hat{b}}^{+}_{\mathbf{r}_\ell}\,|0\rangle\,, \tag{8.79}$$

where $|0\rangle$ is a state with no bosons, while $\hat{\hat{b}}^{+}_{\mathbf{r}_\ell}$ creates a boson at site $\mathbf{r}_\ell$. Thus R stands symbolically for the set $\{\mathbf{r}_\ell\}$ of lattice sites occupied by bosons. In this representation, the iteration Eqn. (8.77) reads

$$\Psi^{(n+1)}\,(R) = \sum_{R'} G(R,\,R')\phi^{(n)}(R'), \tag{8.80}$$

where $G\,(R,\,R')$ are the matrix elements of $\hat{G}$ propagating configuration R' to R,

$$\begin{aligned} G(R,\,R') &= \langle R|[1 - \tau(\mathcal{H} - \hbar\omega)]|\,R'\rangle \\ &= \begin{cases} 1 - \tau\,[U\,(R) - \hbar\omega] & \text{if } R = R' \\ \tau\,\mathcal{J}/2 & \text{if } R \in N(R') \\ 0 & \text{otherwise.} \end{cases} \end{aligned} \tag{8.81}$$

Here $U(R) = \langle R|\mathcal{H}_{\rm pot}|R\rangle$ is the expectation value of the potential energy of this hard-core boson Hamiltonian, and the set $N(R')$ contains all those configurations that can be obtained from R' by moving one of the bosons to any of the available nearest neighbor positions.

In order to introduce Monte Carlo sampling techniques into this iteration scheme, one decomposes $G(R, R')$ into a matrix $P(R, R')$ and a residual weight $W(R')$, $G(R, R') = P(R, R')\, W(R')$ such that

$$\sum_R P(R, R') = 1 \quad \text{and} \quad P(R, R') \geq 0. \tag{8.82}$$

Starting with an initial state $|\phi^{(0)}\rangle$, the probability density after n iterations becomes

$$\begin{aligned}\phi^{(n)}(R) &= \langle R|\hat{G}^n|\phi^{(0)}\rangle \\ &= \sum_{R_0, R_1, \ldots, R_n} \delta_{R, R_n} W(R_{n-1}) W(R_{n-2}) \cdots W(R_0) \\ &\quad \times P(R_n, R_{n-1}) P(R_{n-1}, R_{n-2}) \cdots P(R_1, R_0) \phi^{(0)}(R_0).\end{aligned} \tag{8.83}$$

One defines an n-step random walk on the possible configurations R. With probability $\phi^{(0)}(R_0)$ the Markov chain begins with configuration R_0 and the random walk proceeds as $R_0 \to R_1 \to R_2 \to \ldots R_n$. The transition probability for the move $R_\ell \to R_{\ell+1}$ is given by $P(R_{\ell+1}, R_\ell)$. For each walk the cumulative weight is

$$W^{(n)} = \prod_{\ell=0}^{n=1} W(R_\ell). \tag{8.84}$$

Since the probability for one specific walk is $\prod_{\ell=1}^{n} P(R_\ell, R_{\ell-1}) \phi^{(0)}(R_0)$, one finds that the desired wave function can be constructed as the mean value of the weights $W_k^{(n)}$ averaged over M independent walks labeled by index k,

$$\phi^{(n)}(R) = \lim_{M \to \infty} \frac{1}{M} \sum_{k=1}^{M} W_k^{(n)} \delta_{R, R_{n,k}}. \tag{8.85}$$

As it stands, the algorithm is not very practical since the variance of the estimates increases exponentially with the number of iterations n. However, one can reduce the variance by modifying the scheme through the introduction of a 'guiding wave function' $|\Psi_{\rm G}\rangle$ (Schmidt and Kalos, 1984) which leads to a sort of importance sampling in the iteration process. However, this and other techniques to reduce the variance (Trivedi and Ceperley, 1989), are too specialized to be treated here.

We conclude this section by comparing the results for the order parameter m of the nearest neighbor Heisenberg antiferromagnet on the square lattice (in a normalization where $m = \frac{1}{2}$ for the Néel state): while Eqn. (8.60) yields $m = 0.42$ (Huse and Elser, 1988), Eqn. (8.50) yields $0.32 \leq m \leq 0.36$ (Horsch and von der Linden, 1988; Huse and Elser, 1988; Trivedi and Ceperley, 1989), GFMC yields $0.31 \leq m \leq 0.37$ (Trivedi and Ceperley, 1989), while grand

canonical 'world-line' quantum Monte Carlo (which is based on the Trotter formulation, similar as described in the previous section, and in the end uses an extrapolation to $T \to 0$) yields $m = 0.31$ (Reger and Young, 1988).

8.5 TOWARDS CONSTRUCTING THE NODAL SURFACE OF OFF-LATTICE, MANY-FERMION SYSTEMS: THE 'SURVIVAL OF THE FITTEST' ALGORITHM

Characterizing the groundstate electronic wave function and computing with high accuracy the associated groundstate energy of a many-electron system are fundamental problems for both solid state physics and chemistry (Kohn, 1999; Pople, 1999; Cohen *et al.*, 2012). We have already encountered 'diffusion Monte Carlo' (DMC) as a simulational approach to this problem in which one starts from the observation that the Schrödinger equation can be viewed as a diffusion equation in imaginary time. For a many-particle system the lowest energy wave function is, in general, symmetric with respect to the interchange of the particles and nodeless. Thus, this lowest energy solution would describe a multi-Boson system rather than a multi-Fermion system (which must have an antisymmetric wave function). Thus, solving the diffusion equation in terms of a stochastic process would not yield the required Fermion antisymmetry but would instead converge exponentially fast to the undesired, symmetric solution. The standard method to prevent this 'Boson catastrophe' from occurring is to constrain the propagation of the random walkers by which the stochastic process is realized using the so-called 'fixed node approximation' (Anderson, 1975): the walkers are constrained to propagate only in regions where the wave function has uniform sign. This procedure would be exact if the nodal hypersurface (where the many-body wave function of the Fermionic groundstate changes its sign) were known beforehand, but this is, in general, untrue. Although in favorable cases the fixed-node approximation has yielded acceptable results (as discussed previously), it cannot be systematically improved: thus, this sign problem for many-Fermion problems is still one of the most important stumbling blocks to progress in computational chemistry and physics (Booth *et al.*, 2009).

In the present subsection we consider a methodology by which the exact nodal hypersurface emerges in the course of the simulation (Booth *et al.*, 2009; Cleland *et al.*, 2010). The motivation for this approach comes from the full configuration interaction (FCI) method (Loewdin, 1955) of quantum chemistry: for a small enough number of Fermions, basis sets of quantum systems are considered for which one can obtain the wave function and energy exactly and thus also derive very accurate approximations. The approach unifies Quantum Monte Carlo (QMC) and FCI in such a way that much larger numbers of electrons can be treated. Consequently, not only small molecules can be considered but also problems such as the correlation energy of the homogeneous electron gas (Shepherd *et al.*, 2012) as well as properties

of crystals such as LiH or diamond can be computed with 'chemical accuracy' (Cohen *et al.*, 2012).

This new method performs a long-time integration of the imaginary-time Schrödinger equation, but unlike DMC this is not done in real space but in a space of Slater determinants. While in DMC the propagation step consists both of 'population dynamics' (i.e. walkers are born and die) as well as diffusive displacement moves, in the present algorithm walkers carry a positive or negative sign, and when a pair of walkers of opposite sign coincide on the same determinant they annihilate each other and are removed from the simulation. The walkers represent the instantaneous wave function (unlike FCI where the wave function is represented by amplitude coefficients). Working in Slater determinant space automatically prevents convergence to a bosonic groundstate, since Slater determinants are antisymmetric by construction. Nevertheless, the sign problem persists, since the FCI wave function in this space does not have only positive amplitude coefficients, so in general walkers with both signs will occur.

For simplicity, we do not attempt to describe this algorithm in the most general case but only deal with a specific, but important, example, the homogeneous electron gas. In practice, $N = 54$ electrons in a cubic box with periodic boundary conditions are treated (Shepherd *et al.*, 2012). The Hamiltonian is (setting the electron mass equal to unity)

$$\hat{H} = -\sum_{\alpha} \frac{1}{2}\nabla_{\alpha}^{2} + \sum_{\alpha \neq \beta} \vec{v}_{\alpha\beta} + \frac{1}{2} N v_M, \tag{8.86}$$

where the pairwise potential operator $\vec{v}_{\alpha\beta}$ is the Ewald interaction (Ewald, 1921)

$$\hat{v}_{\alpha\beta} = \frac{1}{V} \sum_{\vec{q}} v_{\vec{q}} \exp[i\vec{q} \cdot (\vec{r}_{\alpha} - \vec{r}_{\beta})], \qquad v_{\vec{q}} = \begin{cases} 4\pi/q^2, & \vec{q} \neq 0, \\ 0, & \vec{q} = 0, \end{cases} \tag{8.87}$$

where V is the real-space unit-cell volume, and v_M is the Madelung term (Ewald, 1921). It represents contributions to the single-particle energy from the Coulomb interaction of a point charge with its own periodic images and with a neutralizing positive charge background (the unit $e = 1$ of elementary charge background has been chosen).

As stressed above, we wish to expand the wave function ψ in a basis of Slater determinants D_i,

$$\psi = \sum_{i} C_i |D_i\rangle. \tag{8.88}$$

For the present problem, each determinant is a normalized, antisymmetrized product of plane waves, $\hat{A}$ being the antisymmetrizing operator,

$$D_i = \hat{A}[\psi_i(\vec{X}_1)\psi_j(\vec{X}_2) \cdots \psi_K(\vec{X}_N)], \tag{8.89}$$

where $\psi_i(\vec{X}) \equiv \psi_j(\vec{r}, \sigma) = \sqrt{V}^{-1} \exp(i\vec{k}_j \cdot \vec{r})\, \delta_{\sigma_j,\sigma}$, σ_j is the spin variable of the electron. The wave vectors $\vec{k}_j$ are chosen to correspond to the reciprocal lattice vectors of a real-space cubic cell of length L,

$$\vec{k} = (2\pi/L)(n, m, l), \tag{8.90}$$

where n, m, l are integers. The Hartree–Fock determinant is the determinant occupying N plane waves with the lowest kinetic energy. The full basis set for the calculation is constructed of all Slater determinants that can be built from $M/2$ plane waves (remember that these are M spin orbitals) forming a closed shell of orbitals in k space up to a cutoff kinetic energy $k_c^2/2$. The single-electron basis set becomes complete only for $k_c \to \infty$, but studying the convergence with M one finds that M of the order of a few hundred to about 2000 is sufficient. This rapid convergence for the electron gas is due to the fact that plane waves are, in fact, natural orbits for the electron gas.

The key step of the method is to use Eqn. (8.88) in the imaginary-time (τ) Schrödinger equation, yielding a set of coupled equations for the determinant coefficient C_i,

$$\frac{-dC_i}{d\tau} = (H_{ii} - S)C_i + \sum_{j \neq i} H_{ij} C_j, \tag{8.91}$$

where the parameter S is called the 'shift'. The straightforward solution of the problem would be to set $dC_i/d\tau = 0$ and solve for S by exact diagonalization and thus obtain the total energy in the chosen basis; however, the size of the Slater determinant space is of the order of $\binom{M/2}{N/2}^2$ for a spin-unpolarized system, a number that grows exponentially with M and N for large M, N, so this straightforward FCI approach is impractical for cases of interest.

The QMC-FCI approach developed by Booth *et al.* (2009, 2012) and Cleland *et al.* (2010, 2012) considers Eqn. (8.91) as a set of master equations for the dynamics of the determinant coefficients in imaginary time, the elements H_{ij} being (non-unitary) transition rates. This dynamic evolution now is simulated by introducing a population of N_w 'walkers' distributed over the determinants, which carry signs to represent the sign of the coefficients within the simulation, $C_i \propto \langle N_i(\tau) \rangle$. The walker population evolves through discretized, imaginary time steps $\delta\tau$ by spawning, death/cloning, and annihilation events according to Eqn. (8.91) until a steady state is reached (Booth *et al.*, 2009; Cleland *et al.*, 2010).

In this formulation, the parameter S is a population control parameter that needs to be updated self-consistently, so the exponential growth of the population settles down at a plateau and S oscillates randomly around the total energy. This energy can also be found in the steady state from (Shepherd *et al.*, 2012)

$$E_{\mathrm{FCIQMC}} = \langle E(\tau) \rangle = \sum_j \langle D_j | \hat{H} | D_0 \rangle \langle N_j(\tau) \rangle / \langle N_0(\tau) \rangle, \tag{8.92}$$

where D_0 is the Hartree–Fock determinant.

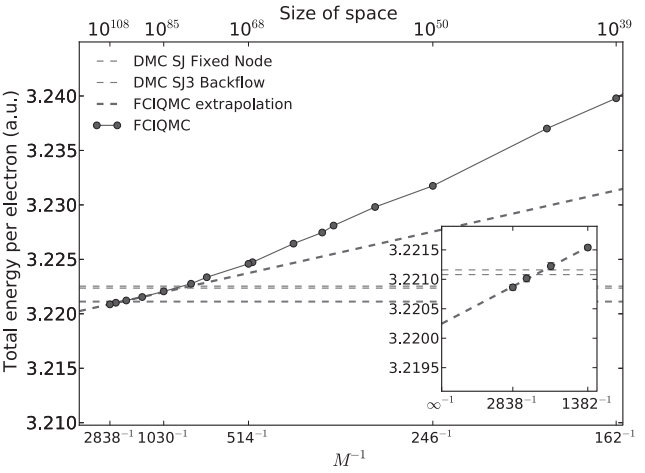

Fig. 8.16 Initiator full configuration interaction Quantum Monte Carlo (i-FCIQMC) total energies for a basis of M spin orbitals for $r_s = 0.5$ a.u. The basis set corresponds to a kinetic energy cutoff with $M = 2838$ Ryd. The calculation used 40 million walkers. The dashed line is a linear extrapolation to $M^{-1} \to 0$ using only the data set with the largest numbers of walkers, shown with error bars in the inset. Several previous estimates are shown for comparison: diffusion Monte Carlo results (DMC) due to Lopez-Rios *et al.* (2006), both according to the fixed node approximation and with the so-called backflow correction. From Shepherd *et al.* (2012).

The 'survival of the fittest-algorithm' (Cleland *et al.*, 2010) introduces one crucial ingredient: the space of determinants is divided instantaneously into those determinants exceeding a population of n_{add} walkers, termed 'initiator determinants', and those that do not exceed this value. When one deals with a determinant whose current population is still zero, in the sum in the second term of Eqn. (8.91) the term describing the net flux of walkers has been spawned from a determinant with an instantaneously population exceeding n_{add}, the child is allowed to survive. However, if the parent walker is at a determinant with a population less than or equal to n_{add}, the child survives *only* if it is spawned to a currently occupied determinant. A typical, useful value is $n_{\text{add}} = 3$ (Shepherd *et al.*, 2012). This 'survival of the fittest criterion' has the effect of dramatically accelerating the convergence of the algorithm. Of course, as the basis set size increases, so does the number of walkers needed to accurately estimate the total energy: while for 200 spin orbitals around 10^6 walkers suffice, for 2000 spin orbits around 10^8 walkers are needed.

While the method described so far is able to yield exact results (in the limit of an infinite number of walkers) for a finite basis set, these results are only upper bounds to the true groundstate energy. This basis-set incompleteness error requires an extrapolation versus $1/M$, and in Fig. 8.16 we see that for $r_s = 0.5$ a.u. the extrapolated value actually is lower, i.e. better, than the best previous estimate (Lopez-Rios *et al.*, 2006). For the (more difficult) case $r_s = 1.0$ a.u. the accuracy of the extrapolated value is comparable to that of the

best previous estimates. (Note that DMC does not involve M as a parameter, and hence DMC estimates are shown as horizontal lines in Fig. 8.16.) Note that the i-FCIQMC results in Fig. 8.16 involve Hilbert spaces ranging from 10^{39} to 10^{108} Slater determinants, sizes that are absolutely unreachable with normal quantum chemistry FCI methods. Although the i-FCIQMC results of Fig. 8.16 had a computational cost of 10^5 core hours (in 2011), i.e. orders of magnitude more than the DMC results shown, the value of the approach described here is that, for the first time, one has an algorithm with systematic improvability (Shepherd *et al.*, 2012).

We have chosen to describe here the application of the i-DCIQMC method to the homogeneous electron gas, because this is the starting point (since the first estimation of its energy by QMC by Ceperley and Alder (1980)) for the widely used local density approximation (LDA) of density functional theory (Kohn, 1999), which still is a standard approach for electronic structure calculation despite its uncontrolled errors (Cohen *et al.*, 2012). But the present technique can be carried over to real problems involving electronic structure calculation in solid state physics. Booth *et al.* (2012) gave an application to the rock-salt structured LiH crystal, obtaining the equation of state (energy versus volume) at $T = 0$ using a $3 \times 3 \times 3$ k-point sampling, again with 54 electrons, using 50 million walkers. Comparing the results to quantum-chemical methods such as Møller–Plesset theory (MP2) (Møller and Plesset, 1934), coupled-cluster singles and doubles (CCSD) (Cizek, 1966) and including perturbative triples (CCSD(T)) (Raghavachari *et al.*, 1989) one finds that i-FCIQMC agrees almost perfectly with the best of these methods, CCSD(T), which deviates from the experimental value only in the meV range. Booth *et al.* (2012) obtained similarly convincing results for a variety of other solids (rare gas crystals like Ne and Ar, other elements such as C and Si, and further compounds such as SiC, LiF, LiCl, BN etc. which crystallize in various structures), and in all cases 'chemical accuracy' (energies accurate to 0.03 eV or better) is achieved. Since the method is somewhat inspired by quantum chemistry, it is no surprise that it is also useful in the traditional application field of quantum chemistry, namely computing energy and structure of small diatomic molecules (e.g. Be_2, C_2, CN, CO, N_2, NO, O_2, F_2), see Cleland *et al.* (2012). But the really exciting perspective of this method is that it probably opens the door to treating strong electronic correlation in solids. A promising first step is the computation of the ferro/antiferromagnetic spin gap of nickel oxide (Booth *et al.*, 2012).

8.6 CONCLUDING REMARKS

In this chapter, we could not even attempt to cover the field exhaustively but rather tried to convey to the reader the flavor of what can be accomplished and how it is done. Of course, many recent variations of the technique have not been described at all, though they are quite important to deal with more

and more problems of solid state physics (such as lattice dynamics beyond the harmonic approximation, electron–phonon coupling, spin–phonon coupling, magnetism, superconductivity, magnetic impurities in metals, hydrogen and other light interstitials in metals, tunneling phenomena in solids, hydrogen-bonded crystals like ice, HF, HCl, etc.). One particularly interesting development has not been dealt with at all, namely the study of quantum dynamical information. As is well known, Monte Carlo sampling readily yields correlations in the 'Trotter direction', i.e. in imaginary time, $\langle \hat{A}(0)\, \hat{A}(\tau)\rangle$. If we could undo the Wick rotation in the complex plane ($it/h \to \tau$) the propagator $\exp(-\tau\mathcal{H})$ would again become the quantum mechanical time evolution operator $\exp(-it\mathcal{H}/h)$. If exact information on $\langle \hat{A}(0)\, \hat{A}(\tau)\rangle$ were available, one could find $\langle \hat{A}(0)\, \hat{A}(t)\rangle$ by analytic continuation; however, in practice this is extremely difficult to do directly because of statistical errors. Gubernatis *et al*. (1991) have shown that using quantum Monte Carlo in conjunction with the maximum entropy method (Skilling, 1989) one can find $\langle \hat{A}(0)\, \hat{A}(t)\rangle$ from $\langle \hat{A}(0)\, \hat{A}(\tau)\rangle$ in favorable cases.

Finally, we would also like to draw the reader's attention to another very promising line of research that we could not cover here, i.e. the application of quantum Monte Carlo methods for the calculation of the electronic structure of molecules and solids (see Foulkes *et al*. (2001) and Grossman and Mitas (2005)). Although computationally intensive, this approach allows the systematic improvement of results via increased sampling.

REFERENCES

Anderson, J. B. (1975), *J. Chem. Phys.* **63**, 1499

Assaad, F. F. and Evertz, H. G. (2008), *Computational Many-Particle Physics*, Lecture Notes in Physics (Springer, Berlin), p. 739.

Badinski, A. and Needs, R. J. (2007), *Phys. Rev. E* **76**, 036707.

Barma, M. and Shastry, B. S. (1977), *Phys. Lett.* **61A**, 15.

Batchelder, D. N., Losee, D. L., and Simmons, R. O. (1968), *Phys. Rev.* **73**, 873.

Beard, B. B. and Wiese, U.-J. (1996), *Phys. Rev. Lett.* **77**, 5130.

Berne, B. J. and Thirumalai, D. (1986), *Ann. Rev. Phys. Chem.* **37**, 401.

Bethe, H. A. (1931), *Z. Phys.* **71**, 205.

Blanckenbecler, R., Scalapino, D. J., and Sugar, R. L. (1981), *Phys. Rev. D* **24**, 2278.

Boninsegni, M., Prokofev, N., and Svistunov, B. (2006a), *Phys. Rev. E* **74**, 036701.

Boninsegni, M., Prokof'ev, N., and Svistunov, B. (2006b), *Phys. Rev. Lett.* **96**, 070601.

Bonner, J. C. and Fisher, M. E. (1964), *Phys. Rev.* **135**, A640.

Booth, G. H., Grüneis, A., Kresse, G., and Alavi, A. (2012), *Nature* **493**, 465.

Booth, G. H., Thorn, A. J. W., and Alavi, A. (2009), *J. Chem. Phys.* **131**, 054106.

Ceperley, D. M. (1995), *Rev. Mod. Phys.* **67**, 279.

Ceperley, D. M. (1996), in *Monte Carlo and Molecular Dynamics of Condensed Matter Systems*, eds. K. Binder and G. Ciccotti (Societá Italiana di Fisica, Bologna), p. 445.

Ceperley, D. M. and Alder, B. J. (1980), *Phys. Rev. Lett.* **45**, 566.

Ceperley, D. M. and Kalos, M. H. (1979), *Monte Carlo Methods in Statistical Physics*, ed. K. Binder (Springer, Berlin), p. 145.
Cizek, J. (1966), *J. Chem. Phys*. **49**, 4256.
Cleland, D., Booth, G. H., and Alavi, A. (2010), *J. Chem. Phys*. **132**, 041103.
Cleland, D., Booth, G. H., Overy, C., and Alavi, A. (2012), *J. Chem. Theory Comput*. **8**, 4138.
Cohen, A. J., Mon-Sanchez, M., and Yang, W. (2012), *Chem. Rev*. **112**, 189.
Cullen, J. J. and Landau, D. P. (1983), *Phys. Rev. B*. **27**, 297.
Dadobaev, G. and Slutsker, A. I. (1981), *Soviet Phys. Solid State* **23**, 1131.
de Raedt, H. and Lagendijk, A. (1981), *Phys. Rev. Lett*. **46**, 77.
de Raedt, H. and Lagendijk, A. (1985), *Phys. Rep*. **127**, 233.
de Raedt, H. and von der Linden, W. (1992), in *The Monte Carlo Method in Condensed Matter Physics*, ed. K. Binder (Springer, Berlin), p. 249.
Doll, J. D. and Gubernatis, J. E. (eds.) (1990), *Qwantwm Simwlations* (World Scientific, Singapore).
Doniach, S., Iuni, M., Kalmeyer, V., and Gabay, M. (1988), *Europhys. Lett*. **6**, 663.
Evertz, H. G. and Marcu, M. (1993), in *Computer Simulations Studies in Condensed Matter Physics VI*, eds. D. P. Landau, K. K. Mon, and H.-B. Schüttler (Springer, Heidelberg).
Evertz, H. G., Lana, G., and Marcu, M. (1993), *Phys. Rev. Lett*. **70**, 875.
Ewald, P. (1921), *Ann. Phys*. **74**, 253.
Feynman, R. P. (1953), *Phys. Rev*. **90**, 1116; 91, 1291; 91, 1301.
Feynman, R. P. and Hibbs, A. R. (1965), *Quantum Mechanics and Path Integrals* (McGraw Hill, New York).
Foulkes, M. W. C., Mitas, L., Needs, R. J., and Rajagopal, G. (2001), *Rev. Mod. Phys*. **73**, 33.
Gillan, M. J. and Christodoulos, F. (1993), *Int. J. Mod. Phys*. **C4**, 287.
Gomez-Santos, G. Joannopoulos, J. D., and Negele, J. W. (1989), *Phys. Rev. B* **39**, 4435.
Grossman, J. C. and Mitas, L. (2005), *Phys. Rev. Lett*. **94**, 056403.
Gubernatis, J. E. and Kawashima, N. (1996), in *Monte Carlo and Molecular Dynamics of Condensed Matter Systems*, eds. K. Binder and G. Ciccotti (Societa Italiana di Fisica, Bologna), p. 519.
Gubernatis, J. E., Jarrell, M., Silver, R. N., and Sivia, D. S. (1991), *Phys. Rev. B* **44**, 6011.
Gull, E., Millis A. J., Lichtenstein, A. I., Rubtsov, A. N., Troyer, M., and Werner, P. (2011), *Rev. Mod. Phys.* 83, 349.
Handscomb, D. C. (1962), *Proc. Cambridge Philos. Soc*. **58**, 594.
Handscomb, D. C. (1964), *Proc. Cambridge Philos. Soc*. **60**, 115.
Hirsch, J. E., Sugar, R. L., Scalapino, D. J., and Blancenbecler, R. (1982), *Phys. Rev. B* **26**, 5033.
Homma, S., Matsuda, H., and Ogita, N. (1984), *Prog. Theor. Phys*. **72**, 1245.
Homma, S., Matsuda, H., and Ogita, N. (1986), *Prog. Theor. Phys*. **75**, 1058.
Horsch, R. and von der Linden, W. (1988), *Z. Phys. B* **72**, 181.
Hubbard, J. (1963), *Proc. Roy. Soc. London A* **276**, 238.
Hulthén, J. L. (1938), *Ark. Mat. Astron. Fjs. A* **26**, 1.
Huse, D. A. and Elser, V. (1988), *Phys. Rev. Lett*. **60**, 2531.
Kalos, M. H. (ed.) (1984), *Monte Carlo Methods in Quantum Problems* (D. Reidel, Dordrecht).
Kasteleijn, P. W. (1952), *Physica* **18**, 104.
Kawashima, N. (1997), in *Computer Simulations Studies in Condensed Matter Physics IX*, eds. D. P. Landau, K. K. Mon, and H.-B. Schüttler (Springer, Heidelberg).
Kawashima, N. and Gubernatis, J. E. (1995), *Phys. Rev. E* **51**, 1547.
Kohn, W. (1999), *Rev. Mod. Phys*. **71**, 1253.

Lee, D. H., Joannopoulos, J. D., and Negele, J. W. (1984), *Phys. Rev. B* **30**, 1599.
Liang, S., Doucot, B., and Anderson, P. W. (1988), *Phys. Rev. Lett.* **61**, 365.
Loewdin, P. O. (1955), *Phys. Rev.* **97**, 1474.
Loh, E. Y., Gubernatis, J. E., Scalettar, R. T., White, S. R., Scalapino, D. J., and Sugar, R. L. (1990), *Phys. Rev. B* **41**, 9301.
Lopez-Rios, P., Ma, A., Drummond, N. D., Fowler, M. D., and Needs, R. J. (2006), *Phys. Rev. E* **74**, 066701.
Lyklema, J. W. (1982), *Phys. Rev. Lett.* **49**, 88.
Manousakis, E. and Salvador, R. (1989), *Phys. Rev. B* **39**, 575.
Marinari, E. and Parisi, G. (1992), *Europhys. Lett.* **19**, 451.
Marshall, W. (1955), *Proc. Roy. Soc. London A* **232**, 64.
Martonak, P., Paul, W., and Binder, K. (1998), *Phys. Rev. E* **57**, 2425.
Marx, D. and Nielaba, P. (1992), *Phys. Rev. A* **45**, 8968.
Marx, D. and Wiechert, H. (1996), *Adv. Chem. Phys.* **95**, 213.
Marx, D., Opitz, O., Nielaba, P., and Binder, K. (1993), *Phys. Rev. Lett.* **70**, 2908.
Miyazawa, S. and Homma, S. (1995), in *Computer Simulations Studies in Condensed Matter Physics VIII*, eds. D. P. Landau, K. K. Mon, and H.-B. Schüttler (Springer, Heidelberg).
Miyazawa, S., Miyashita, S., Makivic, M. S., and Homma, S. (1993), *Prog. Theor. Phys.* **89**, 1167.
Møller, C. and Plesset, M. S. (1934), *Phys. Rev.* **46**, 618.
Müser, M. H. (1996), *Mol. Simulation* **17**, 131.
Müser, M. H., Nielaba, P., and Binder, K. (1995), *Phys. Rev. B* **51**, 2723.
Nho, K. and Landau, D. P. (2004), *Phys. Rev. A* **70**, 053614.
Nielaba, P. (1997), in *Annual Reviews of Computational Physics V*, ed. D. Stauffer (World Scientific, Singapore) p. 137.
Okabe, Y. and Kikuchi, M. (1986), *Phys. Rev. B* **34**, 7896.
Onsager, L. (1944), *Phys. Rev.* **65**, 117.
Ovchinnikov, A. A. (1973), *Sov. Phys. JETP* **37**, 176.
Pople, J. A. (1999), *Rev. Mod. Phys.* **71**, 1267.
Raghavachari, K., Trucks, G. W., Pople, J. A., and Head-Gordon, M. (1989), *Chem. Phys. Lett.* **157**, 479.
Reger, J. D. and Young, A. P. (1988), *Phys. Rev. B* **37**, 5978.
Rutledge, G. C., Lacks, D. J., Martonak, R., and Binder, K. (1998), *J. Chem. Phys.* **108**, 10274.
Sandvik, A. W. (1992), *J. Phys. A* **25**, 3667.
Sandvik, A. W. (1997), *Phys. Rev. B* **56**, 14510.
Sandvik, A. W. (1998), *Phys. Rev. Lett.* **80**, 5196.
Sandvik, A. W. and Kurkijärvi, J. (1991), *Phys. Rev. B* **43**, 5950.
Schmidt, K. E. and Ceperley, D. M. (1992), in *The Monte Carlo Method in Condensed Matter Physics*, ed. K. Binder (Springer, Berlin), p. 205.
Schmidt, K. E. and Kalos, M. H. (1984), in *Applications of the Monte Carlo Method in Statistical Physics*, ed. K. Binder (Springer, Berlin), p. 125.
Shepherd, J. J., Booth, G. H., Grüneis, A., and Alavi, A. (2012), *Phys. Rev. B* **85**, 081103 (R).
Skilling, J. (ed.) (1989), *Maximum Entropy and Bayesian Methods* (Kluwer, Dordrecht).
Suzuki, M. (1966), *J. Phys. Soc. Jpn.* **21**, 2274.
Suzuki, M. (1971), *Prog. Theor. Phys.* **46**, 1337.
Suzuki, M. (1976a), *Commun. Math. Phys.* **51**, 183.
Suzuki, M. (1976b), *Prog. Theor. Phys.* **56**, 1454.
Suzuki, M. (ed.) (1986), *Quantum Monte Carlo Methods* (Springer, Berlin).

Suzuki, M. (ed.) (1992), *Quantum Monte Carlo Methods in Condensed Matter Physics* (World Scientific, Singapore).
Trivedi, N. and Ceperley, D. M. (1989), *Phys. Rev. B* **40**, 2737.
Trotter, H. F. (1959), *Proc. Am. Math. Soc.* **10**, 545.
Troyer, M., Wessel, S., and Alet, F. (2003), *Phys. Rev. Lett.* **90**, 120201.